

Revised manuscript No.: APCATA-D-19-02293R1

<https://doi.org/10.1016/j.apcata.2020.117430>

Methane conversion to ethylene over GaN catalysts. Effect of catalyst nitridation.

Kanchan Dutta¹, Vishnu Chaudhari¹, Chao-Jun Li², Jan Kopyscinski^{1*}

¹ Department of Chemical Engineering, McGill University,

3610 University Street, Montreal, Quebec H3A 0C5, Canada

² Department of Chemistry, McGill University

801 Sherbrooke Street West, Montreal, QC H3A 0B8

* To whom all correspondence should be addressed:

Tel.: +1 514 398 4276

jan.kopyscinski@mcgill.ca

Abstract

Vast availability of natural and shale gases makes methane a reliable source for synthesizing valuable chemical building blocks such as ethylene. A new stable supported GaN/SBA15 catalyst from an emerging class of nitride catalysts was reported for the direct non-oxidative methane coupling to ethylene. The effect of nitridation on the catalyst properties and activity was investigated. The optimum nitridation temperatures were 700 °C and 750 °C for the GaN/SBA15 and the unsupported GaN catalyst, respectively. Supported catalysts were more stable and had 5-10 times higher product (ethylene) formation rates per gram of gallium than the unsupported catalysts due to the higher surface area (>320 vs. <20 m² g⁻¹) and Ga-dispersion inside the pores.

23 Compared to the oxide precursors, the nitrides exhibited a higher atom conversion efficiency for
24 the CH₄ carbon leading to higher ethylene selectivity (71% for GaN/SBA15, <58% for
25 Ga₂O₃/SBA15) and lower coke selectivity (27% for GaN/SBA15, 40% for Ga₂O₃/SBA15).

26

27 **Keywords:** ethylene; direct nonoxidative methane conversion; gallium nitride catalyst;
28 nitridation; SBA-15; catalyst synthesis and characterization.

1 Introduction

The base chemicals for the petrochemical industry like olefins (ethylene, propylene, butadiene) and aromatics (benzene, toluene, and xylenes) are currently derived from oil and natural gas. Estimated to be the world's most widely used petrochemical in terms of production volume, ethylene is the key building block for polyethylene (50%), ethylene oxide (10%) and its derivatives such as ethylene glycol [1]. It is also used to produce vinyl acetate, polyvinyl chloride, polyester fiber and film, and a range of alcohols and solvents. An estimated 60% of total US ethylene production capacity uses liquefied natural gas, with a further 38% derived using naphtha. In 2018, ethylene accounted for 59% of the petrochemical industry revenue in Canada [2], while aromatic hydrocarbons accounted for 38% of revenues in the United States (2017) [1].

Methane (natural gas, shale gas) is considered to be a reliable source for the petrochemical industry. Methane activation and conversion to value-added chemicals are of great interest not only from the fundamental research perspective but also in terms of industrial application as it offers a potential for an alternative route to produce chemicals. Currently, natural gas is converted via the syngas route (indirect and oxidative) to methanol and its derivatives. This conventional syngas route has low efficiency, high capital cost, and associated greenhouse gas emissions. Direct oxidative coupling of methane is another way [3]. However, a significant amount of CO, CO₂, and H₂O are produced, which lowers the product selectivity.

Direct non-oxidative conversion of methane to olefins and aromatics is an alternative and theoretically a very efficient conversion route [4]. However, methane has a very stable C-H bond, which is very difficult to activate under non-oxidative conditions [5]. The review articles from Ma et al.[4], Spivey and Hutchings [6], and Karakaya and Kee [3] summarize the research work that has been conducted with emphasis on metal-modified zeolites. Metals such as Mo, Zn, W, Re,

Cu, Mn, Ni, and Cr have been investigated. Molybdenum-containing zeolites exhibited the highest activity in terms of methane conversion (3-16%) with benzene (50-75%) as the main product [5]. It is hypothesized that an active species on the catalyst surface (i.e., CH_x) is formed, which further dimerizes to produce ethylene. Finally, ethylene is oligomerized and cyclized on the zeolite to form aromatics [4]. A combination of benzene and the active species like CH_2 and CH_3 can form toluene. Two phenyl species (active aryl rings) can form naphthalene [7,8]. Further combination of phenyl species can lead to the formation of polynuclear aromatic compounds (i.e., coke) that deactivates the catalysts, which is the main drawback of this reaction. Adding promoters such as transition metals in Period 4 (Fe, Co, Ni, and Cr) and metals in Group 13 (Ga and Al) show the best improvement in terms of methane conversion, product selectivity, and catalyst stability [4]. It has been shown that Ga containing zeolites are highly active for the dehydrogenation of light alkane [9,10]. But the nature of the active gallium species as well as the gallium alkane intermediates is still under debate. Recently, Dumesic's group developed PtSn-zeolite catalysts that achieved high ethylene selectivities (70-90% at 700 °C, coke not included); yet coking was still a huge problem [11]. They obtained methane conversions (in terms of fraction converted to the products) less than 0.5%, typically 0.25% at 700 °C. Xiao and Varma [12] used bimetallic PtBi-zeolite catalysts and reported ethane (C_2H_6) selectivity of 90% (coke not included) at 700 °C, with methane conversion between 1-5%. However, they had 40-50% coke selectivity with up to 10% ethylene (C_2H_4) selectivity on 1% Pt-0.2% Bi catalyst at 650 °C and 0.1 atm CH_4 partial pressure. They suggested that carbon deposition occurs during the initial activation period. Bajec et al. [13] used Fe/HZSM-5, Mo/HZSM-5, and Fe-Mo/HZSM-5 catalysts for methane activation and coupling to ethane and ethylene. They obtained 1-6% methane conversion, up to 50% ethylene selectivity and 11-35 wt% coke. Their reaction conditions were $T = 700\text{ }^\circ\text{C}$, $\text{WHSV} = 2\text{ h}^{-1}$, $p_{\text{tot}} =$

1.5 bar. Sheng et al. [14] used a less acidic boron-based [B]ZSM-5 catalyst for methane activation and obtained 90% ethylene selectivity (gas phase) with less than 1% methane conversion at 700 °C with an average rate of $0.3 \text{ mmol}_{\text{CH}_4} \text{ h}^{-1} \text{ g}_{\text{cat}}^{-1}$. Low acidity of the support produced more ethylene than benzene and lower coke. Guo et al. [15] synthesized single iron sites embedded in a silica matrix. They reported minimum carbon deposition, maximum ethylene selectivity of 48%, and maximum methane conversion of 48% at 1090 °C.

Almost all the catalysts studied so far were bifunctional precious metals and metal oxides. Our manuscript focuses on metal nitrides, which are gaining interests as heterogeneous catalysts [16]. Nitride catalysts have been used for ammonia synthesis (Co, Mo, Ru nitrides), ammonia decomposition to obtain CO₂ free H₂ (Ru nitride), and for hydrotreating process (Mo nitride) [16]. Nitrides of Si, B have also been used as catalysts support. Compared to the conventional alumina and silica supports, the nitrides can have greater thermal conductivity, increased inertness, modified basicity, and enhanced hydrophobicity [16]. Gallium nitride, a material used in the semiconductor industry, was tested for the first time for methane activation in a batch reactor [17]. The tests were carried out under Ultraviolet (UV) irradiation at room temperature, and also under thermocatalytic conditions at 450 °C and 5-8 h residence time [18,19]. They demonstrated a high selectivity for benzene ($S_{\text{C}_6\text{H}_6} = 97\%$ under UV and $S_{\text{C}_6\text{H}_6} = 89.8\%$, at 450 °C, respectively). However, due to low temperature and thermodynamic limitations, the methane conversion was less than 0.5%. Higher temperatures (>650 °C) and continuous operations are necessary for achieving larger methane conversion [20]. In the optoelectronics and semiconductor industry, GaN is often synthesized in the form of nanostructures (nanotubes, nanowires, and nanorods) through various procedures such as arc discharge, laser ablation, chemical vapor deposition, plasma-assisted molecular beam epitaxy, and metal-organic vapor phase epitaxy. In most of these

procedures, NH_3 at high temperature (nitridation) is used to produce GaN nanostructures from gallium precursors. Some of these methods might not be applicable for the preparation of the catalysts that require a large surface area and well-distributed active sites.

In this work, unsupported catalysts were synthesized, and for the first time, supported gallium nitride catalysts were synthesized, and the effect of the nitridation conditions on the direct non-oxidative methane conversion to value-added chemicals were investigated under flow conditions.

2 Experimental Section

2.1 Catalyst preparation

Two types of catalysts were synthesized; one group was unsupported GaN, the second one was GaN supported on SBA-15 with Ga target loading of 16 wt%. Unsupported catalysts were prepared by the Evaporation Induced Self Assembly (EISA) technique adapted from Chaudhari et al. [21]. Around 1 g of triblock copolymer (Pluronic P-123, Sigma Aldrich) was dissolved in 16 mL of pure anhydrous ethanol (Greenfield Global Inc.) until a homogeneous solution was obtained. This was followed by the addition of 1.7 mL of nitric acid (67-70 wt%, Fisher Scientific) and stirring for complete mixing with the acid. Another solution was prepared in 5 mL DI-water and 5 mL of ethanol with 4.5 g of dry gallium (III) nitrate hydrate powder (99.9998 wt% trace metal basis, ACROS Organic, Thermo Fisher Scientific). DI-water was used to get a homogeneous solution as the nitrate is only slightly soluble in ethanol. The hygroscopic nitrate was always stored under dry inert gas (Ar with < 5 ppm moisture, Praxair) desiccator to prevent moisture absorption. The nitrate bottle was also flushed with Ar after every use. This ensured that the weight of the nitrate was consistent and not influenced by absorbed moisture. The copolymer solution was then added to the gallium precursor solution and stirred for 5 h at 600 rpm at room temperature. The homogeneous, colorless mixture was kept inside a drying oven at 60 °C for 48 h. Thereafter, the

dried copolymer-gallium mixture was calcined at 650 °C for 6 h at a heating rate of 1 °C min⁻¹ in which the copolymer was burned, and the gallium-precursor was converted to Ga₂O₃. Before nitridation, the catalysts were dried for 4.5 h in Ar (99.999%, MEGS Specialty Gases, 15-20 mL_N min⁻¹) at 300 °C with a heating rate of 1 °C min⁻¹ (subscript *N* denotes normal condition with *T* = 0 °C and 1 bar). The nitridation was carried out in a fixed bed reactor with anhydrous ammonia (NH₃, 99.99%, MEGS Specialty Gases, 20 mL_N min⁻¹) flowing top-down through the catalyst bed (around 1 g). A quartz tube (9 mm OD × 7 mm ID × 275 mm long) with a 15-40 μ frit at one end was used as the reactor inside a vertical tube furnace (Mellen Company). At the reactor outlet, the gas was mixed and diluted with Ar. A slipstream was analyzed via mass spectrometry (Pfeiffer Omnistar GSD 301 O1), while the rest was sent through a 10 L hydrochloric acid bubbler (36.5–38 wt%, Fisher Scientific) to absorb unreacted ammonia. Nitridation was carried out at five nitridation temperatures (600, 650, 700, 750 and 800 °C at a heating rate of 1.5 °C min⁻¹ and 24 h NH₃ exposure from the start of heating to cool down), and ammonia exposure time (3-9 h at 750 °C at a heating rate of 1.5 °C min⁻¹). After cooling to room temperature under the NH₃ atmosphere, the reactor was purged with Ar, and the catalyst sample was stored for further use under inert gas in a desiccator.

Supported gallium catalysts were prepared as follows. Ordered mesoporous silica (SBA-15) was synthesized as described in Zhao et al. [22]. Around 4 g of triblock copolymer (Pluronic P-123, Sigma Aldrich) was dissolved by stirring (600 rpm for 5 h) in 95 mL of deionized water until a homogeneous solution was obtained. To this solution, 4 mL of hydrochloric acid was added and stirred for about 15 min at a temperature of 38.5 °C. Then 9.5 mL of tetraethoxysilane (TEOS, 99.9%, Alfa Aesar) was added. The resulting mixture was stirred at 600 rpm for an additional 24 h at 38.5 °C for completing TEOS hydrolysis and precipitation of silica. The above mixture was

placed inside a closed polypropylene digestion DigiTUBEs (SCP science) and kept inside an oven at 100 °C for 48 h for hydrothermal treatment. After cooling down, the white powder was separated by filtration and washed with deionized water several times, followed by overnight drying at 60 °C. Finally, SBA-15 was obtained by calcining the dried solid at 550 °C for 5 h at a heating rate of 1 °C min⁻¹.

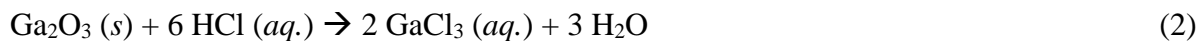
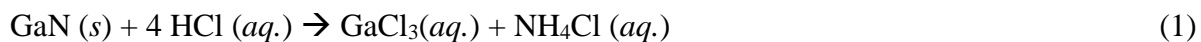
Supported catalysts were synthesized by incipient wetness impregnation of SBA-15 with gallium containing precursor. Typically, 1 g of SBA-15 was impregnated with 1 g of gallium (III) nitrate hydrate in 4.5 mL aqueous solution. The almost wet solid was left for 24 h at room temperature followed by drying overnight at 70 °C. The dried solid was then calcined at 550 °C for 5 h at a heating rate of 1 °C min⁻¹ to produce gallium oxide inside SBA-15. Nitridation of supported catalysts were carried out in the same manner as described above for the unsupported catalysts. Due to the small bulk density, around 200 mg supported gallium oxide (Ga₂O₃/SBA15) was nitridated at temperatures of 650, 700, 750, and 800 °C. Finally, the supported catalysts were stored in Ar filled vials inside the desiccator.

The produced unsupported catalysts were named Ga₂O₃, GaN-750, or GaN-750-03, referring to the calcined and nitridated samples, respectively. In detail, for GaN-750, the 750 denotes the nitridation temperature in degree Celsius (°C) with a total NH₃ exposure of 24 h, while for GaN-750-03, the 03 refers to the nitridation time in hours (e.g., 3, 6 or 9 h). The produced supported catalysts were named Ga₂O₃/SBA15 and GaN/SBA15-750, referring to the calcined and nitridated samples, respectively. In detail, for GaN/SBA15-750, the 750 denotes the nitridation temperature in degree Celsius (°C). N-SBA15-800 refers to a nitridated SBA-15 (without Ga₂O₃) with a nitridation temperature of 800 °C.

2.2 Catalyst characterization

The gallium content in the supported catalysts was determined using Inductively Coupled Plasma - Optical Emission Spectroscopy (ICP-OES, iCAP 6500 dual view Thermo Scientific). The supported catalyst was fused with twice the amount (by weight) of lithium tetraborate (SCP science) in a 9 mL graphite crucible (SCP science). The fusion was carried out in a muffle furnace ramping to 950 °C, where it was held for 30 min. A glassy bead was obtained after cooling down, and the fusion flux was carried out in triplicate. Two different solutions were prepared from the bead; one in 10% HNO₃ (trace metal grade) and another one in 3:1 HCl to HNO₃ concentrated solution (aqua regia). These solutions were digested in polypropylene DigiTUBEs (SCP science) at 95 °C for 2 h until the bead was completely dissolved. After cooling down, the solutions were filtered through 45 µ filter and diluted appropriately for ICP analysis. Unsupported catalysts were either GaN or Ga₂O₃ or a mix of both, and no other metals were present in them. Gallium content in unsupported catalysts can be calculated directly without ICP.

The total nitrogen content of unsupported gallium nitride catalysts was determined by Shimadzu TOC-Vcph with TNM–1 Total Nitrogen Module. Prior to the analysis, around 25-50 mg of the sample was dissolved in 6M hydrochloric acid (HCl) overnight at 80 °C. The gallium nitride was converted to gallium chloride and ammonium chloride, while gallium oxide was converted to gallium chloride and water, as shown in Eqs. (1) and (2), respectively.



The homogenous and clear solution was cooled down, diluted with deionized water to adjust the pH between 2–3. The diluted solution was analyzed for the total nitrogen content. The instrument

was always calibrated before the analysis using ammonium standard (Sigma Aldrich) containing 1000 mg L⁻¹ of N as NH₄⁺ in water. The pH of the calibration solutions was adjusted between 2–3 by using HCl. Ga₂O₃ conversion ($X_{\text{Ga}_2\text{O}_3}$) was calculated based on equation 3 below.

$$X_{\text{Ga}_2\text{O}_3} = \frac{n_{\text{Ga}_2\text{O}_3}^0 - n_{\text{Ga}_2\text{O}_3}}{n_{\text{Ga}_2\text{O}_3}^0} \quad (3)$$

Where, $n_{\text{Ga}_2\text{O}_3}^0 = \frac{(1 - n_N \cdot M_{\text{GaN}})}{M_{\text{Ga}_2\text{O}_3}} + \frac{n_N}{2}$ and $n_{\text{Ga}_2\text{O}_3} = \frac{(1 - n_N \cdot M_{\text{GaN}})}{M_{\text{Ga}_2\text{O}_3}}$, are mol of Ga₂O₃ before and after nitridation (unconverted), respectively. n_N denotes the mol of nitrogen in 1 g of unsupported catalyst determined by total nitrogen analysis, M_{GaN} and $M_{\text{Ga}_2\text{O}_3}$ denote the molar mass of GaN (83.73 g mol⁻¹) and Ga₂O₃ (187.44 g mol⁻¹), respectively. $n_N = \frac{N}{M_N}$, with N as the total nitrogen content in g_N g_{cat}⁻¹ and M_N as the molecular weight of nitrogen (14.01 g mol⁻¹).

This method, however, could not be applied for the supported catalysts because HCl could not leach out gallium salt from the SBA-15 support. Using fusion flux, the silica structure was completely disintegrated, and gallium was completely extracted, but the nitrogen was lost as ammonia gas.

X-Ray Diffraction (XRD) was used to identify the crystallinity of the catalyst. Analyses were conducted on a Bruker D8 Discovery X-Ray Diffractometer with a two-dimensional VANTEC-500 detector and CuK_α ($\lambda = 1.5406 \text{ \AA}$) radiation source. The tube voltage was 40 kV, tube current 20 mA, and scan rate 5° min⁻¹.

Nitrogen adsorption/desorption measurements (–196°C) were conducted using Micromeritics Tristar 3000 BET analyzer to determine total surface area, pore size distribution, and pore volume.

207 Before the analysis, the samples were degassed under vacuum for 12 h at 250 °C. Surface areas
208 of the catalyst were calculated following the BET method.

209 High-resolution transmission electron microscopy (HRTEM) of fresh and spent catalysts was
210 carried out on FEI Tecnai G2 F20 with 200 kV. Prior to the analysis, a catalyst suspension in
211 ethanol was prepared by sonicating 1–2 mg of the catalyst in 2 mL anhydrous ethanol. Energy-
212 dispersive X-ray spectroscopy (EDS) was also carried out for detecting the elements present in
213 the catalyst (qualitative).

214 Scanning Electron Microscopy (SEM) analysis for the unsupported catalyst (Ga_2O_3) was
215 performed using a FEI Inspect F-50 field emission scanning electron microscope. In addition,
216 Energy-Dispersive X-ray Spectroscopy (EDS) experiments were performed for elemental analysis
217 (Ga, N, O, and C).

218 Temperature programmed oxidation coupled with mass spectrometry (TPO-MS) was carried out
219 for the fresh and spent catalysts to estimate the carbon either deposited during methane activation
220 or catalyst synthesis. Around 50 mg of supported catalyst or 250 mg of unsupported catalyst was
221 placed in a quartz tube (9 mm OD \times 7 mm ID \times 275 mm long and 15-40 μ frit) and heated in the
222 presence of air (Ultra Zero Air, MEGS Specialty Gases, 22 mL_N min⁻¹) to 950 °C with a heating
223 rate of 5 °C min⁻¹. The product gas at the reactor outlet was electrically heated to 200 °C, mixed
224 with Ar (MEGS Specialty Gases, 10 mL_N min⁻¹), and then subsequently analyzed by a mass
225 spectrometer (Pfeiffer Omnistar GSD 301) calibrated for CO₂ (m/z = 44). The gas flow rates were
226 controlled by respective calibrated Vögtlin red-y smart controllers (\pm 0.3 % accuracy,
227 Switzerland).

In addition, temperature-programmed oxidation with thermogravimetric analysis (TPO-TGA) was carried out for both fresh and spent catalysts (Q500 TA Instrument). 20–25 mg of catalyst was first purged for 30 min with N₂ at room temperature to remove air from the system and then heated at the rate of 5 °C min⁻¹ to 120 °C to remove the moisture. After a holding for 30 min at 120 °C, the sample was then heated to 950 °C at 5 °C min⁻¹ in the presence of air and held at 950 °C for 30 min, while the weight change was recorded.

Catalyst synthesis (both unsupported and supported) and the subsequent analyses (BET, XRD, ICP) were repeated for confirming repeatability and reproducibility.

2.3 Catalytic activity measurements

The catalyst performance was measured in a vertical packed bed reactor at 700 °C and 1 bar_{abs}. A quartz tube (9 mm OD × 7 mm ID × 335 mm long) with a 15–40 μ frit at one end was used as the reactor inside a vertical tube furnace (Mellen Company). Around 500 mg of unsupported or 100 mg of supported catalysts were loaded in order to achieve the same bed height of 11 ± 1 mm and the same residence times of 1.3 s (superficial gas velocity at 700 °C) for both catalysts. The bulk densities of the GaN and GaN/SBA15 were 1300 kg m⁻³ and 260 kg m⁻³, respectively. The inlet gas contained 80 vol% CH₄ (99.999%, Praxair) in Ar (99.999%, MEGS Specialty Gases), which were mass flow controlled using calibrated Vögtlin red-y smart controller (± 0.3% accuracy, Switzerland). The resulting CH₄-based gas hourly space velocities (GHSV) were the same for both GaN and GaN/SBA15 with a value of 567 h⁻¹. The reactor outlet and transfer lines were electrically heated at 200 °C to avoid condensation of the organic components (i.e., C₆H₆, C₇H₈, C₁₀H₈). A quadrupole mass spectrometer (Pfeiffer Omnistar GSD 301) was used for product gas analysis; the instrument was calibrated for methane (CH₄), ethylene (C₂H₄), propylene (C₃H₆), benzene (C₆H₆), toluene (C₇H₈), naphthalene (C₁₀H₈), carbon dioxide (CO₂) and hydrogen (H₂)

with argon (Ar) as the internal standard (additional details are in the supplementary information). The calibration of the mass spectrometer was verified by a calibrated gas chromatograph (SRI GC 8610) for CH₄, H₂, and C₆H₆ (Fig. S1).

Prior to heating, the catalyst was purged with Ar (25 mL_N min⁻¹) for 1 h, then heated to 700 °C at a rate of 5 °C min⁻¹, and subsequently, CH₄ was added. The internal reactor temperature (i.e., within the catalyst bed) was measured by a K-type thermocouple (Omega), which was used to control the furnace.

Based on a detailed mass spectrum analysis and calibration factors, the CH₄ conversion, the product molar flow rates (μmol min⁻¹ g_{Ga}⁻¹) as a function of time on stream were determined (Fig. 6 and 7). Besides ethylene (C₂H₄), other hydrocarbons such as propylene (C₃H₆), benzene (C₆H₆), toluene (C₇H₈) and naphthalene (C₁₀H₈; see Fig. S16) were detected and quantified. The CH₄ conversion was calculated based on the gaseous carbon products (equation 4).

$$x_{CH_4} = \frac{\sum v_i \cdot \dot{n}_i}{\dot{n}_{CH_4, in}} \times 100 \quad (4)$$

Where \dot{n}_i denotes the molar flow rate in μmol min⁻¹, while v_i denotes the number of carbon atoms in the i^{th} species in the product stream (i.e., C₂H₄, C₃H₆, CO₂, C₆H₆, C₇H₈, and C₁₀H₈). The denominator represents the molar flow of methane in the feed (μmol min⁻¹). The conversion closely represents the percentage (%) of carbon (C) converted to hydrocarbons and not coke. Results reported in this work for the methane activation were consistent within 5% of C and H elemental balances.

Reactivity experiments were repeated with the catalyst prepared from the same as well as from different batches. The unsupported catalysts showed good repeatability and reproducibility, as illustrated in Fig. S2A and B. The supported catalysts exhibited a slightly larger deviation for

different catalyst batches (Fig. S2C and D) that could be attributed to the incipient wetness impregnation step, which is limited by slower redistribution of Ga inside the pores.

3 Results and discussion

3.1 Nitridation of unsupported catalysts

The nitridation study for unsupported catalysts was divided into two parts, to investigate (1) the effect of nitridation temperature, and (2) the effect of NH_3 exposure time at a fixed temperature (750 °C). In the first part, the temperature was increased under the NH_3 atmosphere, while in the second study, NH_3 was added after the target temperature of 750 °C was reached (under Ar atmosphere). During the nitridation, water is produced ($\text{Ga}_2\text{O}_3 + 2 \text{NH}_3 \rightleftharpoons 2 \text{GaN} + 3 \text{H}_2\text{O}$), which was recorded by mean of mass spectrometry (H_2O , $m/z = 18$). The first study was a combination of a temperature-programmed reaction with an extended soak time at five different temperatures to determine the onset and peak temperature for the Ga_2O_3 nitridation and the optimum condition. The results clearly indicate that the nitridation started above 600 °C and that the maximum H_2O formation rate was close to the targeted nitridation temperature for $T_{\text{Nit}} = 650\text{-}800$ °C (Fig. 1A). No maximum was observed for 600 °C, indicating a very slow nitridation rate. For nitridation temperatures of 750 and 800 °C, the water signal dropped after 8-10 h to the same level resulting in a very similar Ga_2O_3 conversion, which was confirmed by the total nitrogen analysis ($\sim 88 \pm 5\%$, Fig. 1A and B).

For GaN-650 and GaN-700, the water production rate (i.e., Ga_2O_3 conversion rate) was significantly slower, and even after a total NH_3 exposure time of 24 h, the Ga_2O_3 conversions were $46 \pm 5\%$ and $70 \pm 5\%$, respectively (Fig. 1B). XRD analyses confirmed the trend as a distinct transition from $\beta\text{-Ga}_2\text{O}_3$ to GaN with increasing nitridation temperature was observed (Fig. 1C).

The catalyst nitrated at 600 °C exhibited predominately broad XRD pattern of β -Ga₂O₃ ($2\theta = 31.7^\circ, 35.2^\circ, 38.4^\circ, \text{ and } 64.7^\circ$; PDF file #00-006-0523 from the International Centre for Diffraction Data). The XRD pattern for the samples treated at 650 °C started to show clear diffraction pattern of GaN ($2\theta = 32.5^\circ, 36.9^\circ, \text{ and } 57.9^\circ$; PDF file # 04-013-1733) with only minor peaks for β -Ga₂O₃. At nitridation temperatures of 700 °C and higher, the catalyst samples had only diffraction patterns corresponding to GaN, even though the Ga₂O₃ conversion was only between 70-90%.

Based on this result, a nitridation temperature of 750 °C was sufficient as complete bulk conversion might not be necessary for the methane conversion. The nitridation reaction is thermodynamically unfavorable and highly endothermic as indicated by the large positive standard Gibbs free energy and heat of reaction ($\Delta G_{R,298K} = 191.8 \text{ kJ mol}^{-1}$ and $\Delta H_{R,298K} = 238.2 \text{ kJ mol}^{-1}$) [23]. However, the significant excess of ammonia, the removal of gaseous products (water), and higher temperatures (750 and 800 °C) resulted in an 88% conversion of Ga₂O₃ to GaN (Fig. 1B). For lower temperatures (with the same gas flow rates), the Ga₂O₃ conversion was significantly smaller (by around 50%), indicating that more time and/or higher temperature was needed. Moreover, not all Ga was accessible for NH₃ due to collapsing of the pores.

In the second study, the Ga₂O₃ samples were exposed to NH₃ for 3 h, 6 h, or 9 h after the desired nitridation temperature of 750 °C was achieved. The results are illustrated in Fig. 1D, E, and F. The H₂O signal increased instantaneously at the onset of the nitridation and then declined rather fast with time. The longer the nitridation time, the smaller the H₂O signal, and the higher the Ga₂O₃ conversion (i.e., 64% at 3 h vs. 85% at 9 h, see Fig. 1D and E). XRD analyses of these three samples showed only diffraction patterns corresponding to GaN (Fig. 1F). Even with a Ga₂O₃

conversion of only 64% at 3 h NH_3 exposure time, the peaks corresponding to oxide ($\beta\text{-Ga}_2\text{O}_3$) were not visible. It has been suggested that the conversion of $\beta\text{-Ga}_2\text{O}_3$ to GaN proceed either through the formation of amorphous gallium oxynitride (GaO_xN_y) intermediates or via Ga_2O [24]. The latter Ga_2O as gas phase intermediate is assumed at temperatures higher than 900 °C.

Nitrogen adsorption/desorption analysis of all unsupported Ga_2O_3 and GaN catalysts exhibited type-IV isotherms with H3 and H4 type hysteresis loops with bimodal pore size distribution (Fig. S3). The disordered structure was also observed for Ga_2O_3 synthesized by the EISA method [25]. Table 1 summarizes BET surface areas and pore volumes, as well as two pore sizes with the highest contributions. The Ga_2O_3 had a surface area of $19 \text{ m}^2 \text{ g}^{-1}$ and a pore volume of $0.08 \text{ cm}^3 \text{ g}^{-1}$ with a bimodal pore size distribution of 7.5 and 31.5 nm. More than 85% of the surface area corresponded to meso- and macropores, while the rest were micropores.

Upon nitridation at 650 °C, the surface area decreased by ~20% down to $15 \text{ m}^2 \text{ g}^{-1}$ with a pore volume of $0.075 \text{ cm}^3 \text{ g}^{-1}$. This was probably due to the change from the monoclinic crystal structure of $\beta\text{-Ga}_2\text{O}_3$ to the wurtzite structure of GaN. A further decrease of the surface area to $11 \text{ m}^2 \text{ g}^{-1}$ at $T_{\text{Nitridation}}$ of 800 °C could be attributed to sintering and/or pore structure collapse due to the crystallization of GaN at temperatures above the calcination temperatures [26]. Commercial GaN powder had a slightly smaller surface area with $S_{\text{BET}} = 8 \text{ m}^2 \text{ g}^{-1}$ than catalyst prepared in this work [20].

TEM and EDS analysis for Ga_2O_3 and GaN-650 are illustrated in Fig. 2. Both gallium catalysts are an agglomeration of nanoparticles with polycrystalline structure, as depicted with the darkfield in the top-left insets of Fig. 2A and B. The nanoparticle size ranges from 20 to 200 nm (Fig. S4). Polycrystalline Ga_2O_3 has several characteristic d-spacings representing the monoclinic structure

(cell dimensions of $a = 12.23 \pm 0.02$, $b = 3.04 \pm 0.01$, $c = 5.80 \pm 0.01$ Å and $\beta = 103.7 \pm 0.3^\circ$)[27]. Fig. 2 and S5 visualizes d-spacings of 3.0 ± 0.1 and 6.0 ± 0.1 Å corresponding to the [001] plane [28] as well as 9.9 Å associated with the [010] plane [29].

The synthesized GaN-650 catalyst had a Ga₂O₃ conversion after the nitridation of around 46 %; thus, as expected, both GaN and Ga₂O₃ phases were visible in the TEM, with a possible core-shell structure of Ga₂O₃ in the center (Fig. 2B and S6). GaN has a regular wurtzite structure with both *m*- and *c*-planes. The *m*-plane is non-polar and made of alternating Ga and N ions, while the *c*-plane is polar containing either Ga or N ions. The lattice parameters of the *m*-plane with 5.2 Å, as well as the hexagonal structure of the *c*-plane with $\sqrt{3}a = 5.5$ Å could be observed, as illustrated in Fig. 2B and Fig. S7, respectively. For the amorphous Ga₂O₃ part, a *d*-spacing of 9.9 Å was measured. An amorphous gallium oxynitride (GaO_xN_y) might exist at the boundary between GaN and Ga₂O₃.

Fig. 2C depicts the EDS for fresh Ga₂O₃, and fresh and spent GaN-650 catalysts. As expected, the pure Ga₂O₃ sample had no peaks corresponding to nitrogen and much higher oxygen counts than both of the GaN-650 samples (fresh and spent) that contain GaN as well as Ga₂O₃ phases. The spent GaN catalyst had a higher carbon peak and, consequently, smaller peaks associated with nitrogen and oxygen, confirming the presence of carbonaceous material deposition. Some contributions to the carbon signal and all the copper count were from the sample grid. The EDS data shown were normalized based on the gallium count and semi-quantitative in nature.

3.2 Nitridation of supported catalysts

Supported gallium oxide (Ga₂O₃/SBA15) samples showed a slightly higher H₂O signal upon nitridation when compared with SBA-15 without gallium oxide (GaN/SBA15 vs. N-SBA15 in

Fig. 3A). But no maximum was observed, which was probably due to the lower Ga₂O₃ content (around 35 mg compared to 1000 mg for the unsupported Ga₂O₃ loaded for nitridation). As mentioned above, the degree of nitridation (i.e., Ga₂O₃ conversion) by total nitrogen analyses of the product (GaN/SBA15) could not be determined.

The nitridated gallium-containing supported catalysts showed the presence of crystalline GaN but did not exhibit any peak corresponding to β -Ga₂O₃ (Fig. 3B). Even for the Ga₂O₃/SBA15 samples, no diffraction pattern for β -Ga₂O₃ was observed, indicating very small non-crystalline particles.

The XRD peak around $2\theta = 44^\circ$ (Fig. 3B) corresponds to the aluminum sample holder of XRD.

Although the total N could not be performed for the supported catalysts, the peaks corresponding to the nitrides are sharper at all nitridation temperatures compared to the unsupported catalysts (GaN-600 and 650). Since the total Ga content in the supported catalyst was much lower, it can be assumed that the conversion of Ga₂O₃ to GaN was near completion for all samples.

The prepared support SBA-15 had a total BET surface area of 912 m² g⁻¹ (~20% micro and ~80% mesopores), which decreased to 420 m² g⁻¹ (~15% micropores) when nitridated at 800 °C (N-SBA15-800). This might be due to partial pore collapse at higher temperatures, as shown by the reduced pore volume (i.e., from 0.89 to 0.61 cm³ g⁻¹). Adding Ga to the support (including impregnation and calcination at 550 °C) also reduced the total surface area to 426 m² g⁻¹ and pore volume to 0.53 cm³ g⁻¹ but did not change the average pore size (Table 2). Moreover, the data show that the share of the micropore surface area decreased from 20% to 13%.

The surface areas of Ga₂O₃/SBA15 was still 20 times larger than for the unsupported catalyst samples with a value of 19 m² g⁻¹ (see Ga₂O₃ in Table 1). Thus, it was easier for NH₃ to access Ga₂O₃ resulting in most likely in a higher conversion during the nitridation, especially at lower temperatures.

Upon nitridation up to 700 °C, the surface area did not change much, but the average pore size decreased from 7.9 to 6.4 nm when compared to the Ga₂O₃/SBA15 sample. An increase in the nitridation temperature above 750 °C (i.e., GaN/SBA15-750 and 800) resulted in the reduction of the total surface area down to 320 m² g⁻¹. The share of micropores decreased even further to 8%. At higher nitridation temperatures, the surface area reduction was most likely due to a combination of sintering of GaN particles and pore structure collapsed [26].

Compared to the unsupported catalyst (GaN), the supported catalysts (GaN/SBA15) had a unimodal pore size distribution at around 6.4 nm (Table 2, Fig. S9).

Based on ICP analyses, Ga-loadings of 13 ± 1 wt% in Ga₂O₃/SBA15 (target 16 wt% Ga) and 11 ± 1 wt% in GaN/SBA15 were determined. The loss of around 3 wt% from the target loading could be attributed to the loss of gallium nitrate solution during catalyst synthesis.

HRTEM was carried out for Ga₂O₃/SBA15, GaN/SBA15-650, and GaN/SBA15-800 catalysts, both fresh and spent (Fig. 4 and Fig. S10). For the fresh Ga₂O₃/SBA15, no gallium nanoparticles were observed, while the ordered hexagonal pore structure of the SBA-15 was clearly visible with a size of around 8 nm (same as determined by BET measurement see Table 2). In EDS, however, the presence of Ga was confirmed (Fig. 4D). This suggests that the Ga₂O₃ nanoparticles were highly amorphous as supported by XRD results for the Ga₂O₃/SBA15 (Fig. 3B). GaN, on the other hand, was clearly distinguishable from the SBA-15 in the TEM, as depicted in Fig. 4B and C for GaN/SBA15-650 and 800, respectively. Moreover, Fig. 4B and C show clearly that the GaN nanoparticles (3-5 nm, Fig. 4 B and C) were inside the 6-8 nm pores of the SBA-15 support. XRD measurement confirmed that GaN had a crystalline structure (see Fig. 3B).

Although the spent GaN/SBA15-800 did not show much change in morphology, several agglomerations of particles inside the hexagonal array of pores for the spent GaN/SBA15-650

were observed with the TEM (see Fig. S10B). These agglomerations were most likely carbon deposition due to coking during the methane conversion. EDS analysis (Si normalized) confirmed that the spent GaN/SBA15-650 catalyst had a much higher carbon count than the fresh catalyst (Fig. 4D). Consequently, the peak corresponding to Ga was significantly smaller in the spent than in the fresh catalyst.

3.3 Activity measurements over unsupported catalysts

Mass spectrum analyses revealed that the Ga_2O_3 sample produced amount of H_2O ($m/z = 18$) and CO_2 ($m/z = 44$) in the first hour during the methane activation (Fig. 5A to D), while the nitridated catalysts did not exhibit any formation of H_2O and CO_2 (Fig. 5E to H and Fig. S11 for GaN-750). The GaN-600 sample showed an insignificant amount of H_2O and CO_2 , (see Fig. S12), even though this sample contained ~65% of Ga_2O_3 . This may indicate that during the nitridation, mostly the outer surface of the low porosity Ga_2O_3 was converted to GaN, while the bulk remained Ga_2O_3 (core-shell structure).

This also explains the different behavior of the H_2 formation ($m/z = 2$) for the Ga_2O_3 (max. H_2 at 2 h) and GaN (max. H_2 at < 1 h) samples. During the induction period, CH_4 produced H_2O , CO, and CO_2 on Ga_2O_3 , creating an oxygen vacancy in the crystal lattice, also predicted by our DFT work [21]. SEM-EDS analysis of fresh and used Ga_2O_3 catalysts (Fig. S13 and S14) showed only a marginal loss of oxygen within the error of estimation. Also, the XRD for fresh and spent Ga_2O_3 were practically indistinguishable, indicating no change in the crystal structure (Fig. S15).

Since CO and C_2H_4 have the same nominal mass ($m/z = 28$), it was impossible to distinguish between them via mass spectrometry. CO and CO_2 might have been formed via gallium-methoxy species (Ga-O-CH_3) that were experimentally observed via ^{13}C NMR over Ga-modified zeolites [10]. However, the number of methoxy groups are assumed to be much smaller than the gallium-

430 methyl species. The reaction pathway towards CO and CO₂ has been reported by Chaudhari et
431 al.[21]. It has been shown that gallium oxide is active towards the reverse water-gas shift reaction
432 during the alkane dehydrogenation in the presence of CO₂ [30]. Assuming the reverse water-gas
433 shift reaction at equilibrium, the maximum CO formation and hence the minimum C₂H₄ formation
434 rates could be determined. Since negligible amounts of H₂O and CO₂ were observed for the
435 nitridated samples, the mass-to-charge ratio $m/z = 28$ was associated with C₂H₄ only (Fig. 5E to
436 F).

437 All unsupported catalyst samples exhibited similar behavior in terms of CH₄ conversion as well
438 as product formation rate except ethylene. The ethylene rates were higher for the nitridated
439 catalysts when compared with the oxide precursor (Ga₂O₃), but the rates were similar within the
440 nitridated samples from 600-800 °C. At the onset of the reaction, CH₄ conversion values of 4%
441 were determined, which rapidly decreased to less than 1% after 3 h on stream. The steady-state
442 rate attained was up to 0.1 mmol_{CH₄} h⁻¹ g_{Ga}⁻¹.

443 C₂H₄ had the highest hydrocarbon-based formation rate at the beginning of the reaction with up
444 to 5 μmol min⁻¹ g_{Ga}⁻¹ that was 3 to 4 orders of magnitude larger than for the other hydrocarbons.
445 Benzene formation rates were about 100 times smaller, while the rates for propylene, toluene, and
446 naphthalene (Fig. S16) were more than 1000 times lower. The maximum hydrocarbon and H₂
447 formation rates for the nitridated catalysts occurred within the first hour, while the non-nitridated
448 catalyst (Ga₂O₃) had longer induction time with an observed maxima between 1 and 2 h (Fig.
449 6 and 7).

450 Independent of the nitridation temperature and time, all unsupported catalysts deactivated faster
451 within 3-5 h due to coking (Fig. 6 and 7), which was evident from the color change from yellow
452 (fresh GaN) or white (fresh Ga₂O₃) to black (spent, Fig. S17) as well as the temperature-

programmed oxidation results (see below). The degree of nitridation influenced slightly more the formation rates of aromatic compounds (C_6H_6 and C_7H_8) than of olefins (C_2H_4 and C_3H_6). The Ga_2O_3 catalyst had the lowest C_6H_6 and C_7H_8 formation rates, followed by the catalyst nitridated 600 °C (GaN-600). GaN-700 and GaN-750 exhibited the highest C_6H_6 and C_7H_8 formation rates. If C_2H_4 would be the only hydrocarbon product, the ratio of the observed H_2 to C_2H_4 formation rates should be 2, corresponding to the stoichiometric factor shown in equation 5.



For the unsupported catalysts, the ratio of hydrogen and ethylene formation rate changed with time, as illustrated in Fig. S18A and B. At the onset, the ratio was close to two, while it increased to a maximum of 7-12 depending on the catalyst after 1 to 2 h on stream. Afterward, the ratio attained a value of 3 at the end of the run. The ratio was higher than 2; thus, more H_2 was formed, indicating that a considerable amount of hydrocarbons were adsorbed on the catalyst surface as CH_x^* or $C_yH_z^*$ species with a yet unknown stoichiometry. Since the C_2H_4 formation rate was a factor of 100 to 1000 larger than the other gaseous hydrocarbons, they would not influence the observed H_2/C_2H_4 ratio significantly. No methane activation was observed when the reaction was carried out in an empty quartz reactor (blank experiments); therefore, homogeneous gas phase reactions were negligible at 700 °C.

A single CO_2 peak at 467 ± 5 °C for the spent Ga_2O_3 was observed during temperature-programmed oxidation (TPO-MS), which shifted slightly to higher temperatures 480 ± 6 °C for the GaN catalysts as illustrated in Fig. 8. A H_2O peak ($m/z = 18$) was observed at the same temperature (Fig. S19A). Based on this temperature range, it can be assumed that the carbonaceous material was rather amorphous instead of graphitic carbon, which requires higher

oxidation temperatures [31]. In addition, the single CO₂ peak indicates a single carbon surface species that behaved similarly on the GaN and Ga₂O₃ samples under an oxidizing atmosphere. TPO-TGA measurements of the spent samples confirmed the results, as depicted in Fig. S20A and B. Interestingly, at temperatures above 550 °C the weight of the used GaN samples increased due to the oxidation to Ga₂O₃, which was also observed in our previous study [20].

The quantitative analysis of the spent catalyst after 5 h yielded a relative carbon amount of 22 mg g_{cat}⁻¹ for Ga₂O₃ and 10-16 mg g_{cat}⁻¹ for GaN catalysts (Table S1).

Based on the TPO analysis and product gas composition data, the overall selectivities for the adsorbed carbon as well as specific selectivities and total C₂H₄ yield were determined and summarized in Table 3. It is evident that the adsorbed carbon/coke, yet with an unknown C_xH_y stoichiometry, was the primary product, whereas the total hydrocarbon selectivity was between 30-50 mol%. The hydrocarbons itself were predominately C₂H₄ with selectivity values of up to 49 mol% for GaN-750-03 and 27 to 34 mol% for Ga₂O₃. For the latter, a range was calculated indicating the minimum and maximum value for C₂H₄ selectivity depending on the influence of the reverse water-gas shift reaction and thus CO formation. C₆H₆ and C₃H₈ selectivities ranged from 0.5 to 0.9 mol% and 0.1 to 0.3 mol%, respectively.

To put these results in context, the equilibrium composition was calculated with the assumption of CH₄ as the only reactant and H₂, C₂H₄, and C₃H₆ as the only products. Aromatic compounds benzene, toluene, and naphthalene being less than 100 times than C₂H₄ had not been considered in the calculations. Thermodynamically, the maximum CH₄ conversions and C₂H₄ yields (without coke) are 4.1% and 3.5% at 700 °C, 9.1%, and 8.1% at 800 °C and 17.0% and 15.5% at 900 °C, respectively (see Fig. S21). Carbon deposition was excluded from the conversion calculations (Fig. 6) as the molar rates of surface intermediates were not measured as a function of time.

Methane conversion based on carbon incorporated in the products (excluding coke) can be compared with the equilibrium calculations (Fig. S21). The equilibrium calculations did not include coke. The steady-state conversion (Fig. 6) was less than 10% of the equilibrium conversion (Fig. S21).

3.4 Activity measurements over supported catalysts

Unlike unsupported Ga_2O_3 catalyst, the supported $\text{Ga}_2\text{O}_3/\text{SBA15}$ sample produced H_2O and CO_2 in the first hour on stream, while the nitridated catalysts did not produce a significant amount of CO_2 and H_2O (Fig. 9 and Fig. S22).

The main hydrocarbon product of the supported catalysts was again ethylene (C_2H_4), as depicted in Fig. 10. Supported GaN catalysts were very selective for the direct non-oxidative methane dehydrogenation and subsequent coupling to ethylene. Propylene and benzene were approximately 100 and 1000 times smaller, respectively. Unlike the unsupported catalyst, the initial CH_4 conversion was less than 1%, and then decreased to less than 0.5%, and remained steady (Fig. 10A). Similar CH_4 conversions ($< 0.3\%$) were reported by Dumesic's group over PtSn-zeolite catalysts [32]. The supported GaN/SBA15 deactivates slower than the unsupported GaN, at the initial reaction stage. The steady-state rate attained was between $1.5\text{-}3.0 \text{ mmol}_{\text{CH}_4} \text{ h}^{-1} \text{ g}_{\text{Ga}}^{-1}$ (equivalent to $0.2\text{-}0.4 \text{ mmol}_{\text{CH}_4} \text{ h}^{-1} \text{ g}_{\text{cat}}^{-1}$), which was at least 10 times the unsupported catalysts. The rate is comparable to the rate reported by Sheng et al. [14] with $0.3 \text{ mmol}_{\text{CH}_4} \text{ h}^{-1} \text{ g}_{\text{Cat}}^{-1}$.

The supported catalysts were more stable than the unsupported. Moreover, the C_2H_4 and C_3H_6 formation rates per gram of Ga were about 10 and 100 times higher for the supported catalyst (Fig. 6 vs. 10), respectively. The supported catalyst had more than 20 times higher porosity than the unsupported samples (see Tables 1 and 2). Moreover, GaN within the SBA-15 structure was very

well dispersed with a crystallite size of 3-5 nm (from Fig. 4 B and C), whereas the unsupported GaN consists of an agglomeration of nanoparticles with 20–200 nm (Fig. S4). The latter had a much lower Ga dispersion and, therefore, a much lower rate per mass of gallium. It seems that methane coupling to ethylene over GaN is structure sensitive.

After approximately 1 h, the CH₄ conversions were in steady-state and corresponded to the hydrocarbon formation rates (specifically C₂H₄). This indicates that the active catalyst surface might have been covered with CH₄ during the initial phase, which has been confirmed by TGA experiments, as reported in our work [33]. This was also suggested by Xiao and Varma [12].

The Ga₂O₃/SBA15 and GaN/SBA15-650 exhibited higher CH₄ conversions compared to the samples nitridated at 700 to 800 °C (GaN/SBA15-700 to GaN/SBA15-800, Fig. 10A). However, the H₂ formation rate differs significantly. For Ga₂O₃/SBA15, the H₂ production rate increased from 43 to 68 μmol min⁻¹ g_{Ga}⁻¹ within 7 h of reaction time. At the same time, the H₂O formation decreased (Fig. S22). Since no water was produced over the nitridated samples, the H₂ formation rates were constant with GaN/SBA15-650 achieving the fastest rate of ~110 μmol min⁻¹ g_{Ga}⁻¹ and GaN/SBA15-700 the slowest rate of ~40 μmol min⁻¹ g_{Ga}⁻¹. The C₂H₄ production rate exhibited a similar trend as observed for H₂, highest steady-state rate of 22 μmol min⁻¹ g_{Ga}⁻¹ for GaN/SBA15-650, and lowest of 12 μmol min⁻¹ g_{Ga}⁻¹ for GaN/SBA15-700. Minor components such as C₃H₆, C₆H₆, and C₇H₈ were 100–1000 times lower than C₂H₄, similar to their unsupported counterparts.

The ratio of the H₂ and C₂H₄ formation rates over the supported samples were close to three and did not change significantly with time on stream (Fig. S18C). This value was much smaller than for the unsupported gallium catalysts indicating that over supported gallium catalysts less adsorbed carbon surface species (i.e., CH_x*) were formed. Since the behavior for the unsupported

and supported GaN catalysts were different (i.e., supported catalyst was more stable), it is assumed that the adsorbed carbonaceous species was not catalytically active.

Temperature programmed oxidation - mass spectrometry (TPO-MS) analyses of the spent catalysts showed a major CO₂ peak at 600 ± 10 °C, as illustrated in Fig. 11. This was around 120 °C higher than for the unsupported catalysts (Fig. 11 vs. 8). The same behavior was observed by means of thermogravimetric experiments (TPO-TGA, Fig. S20) as well as by determining the produced water via mass spectrometry (Fig. S19). For the latter, the H₂O signal corresponded perfectly to the CO₂ peaks. The reason for the higher temperature might be the confinement effect due to the small pore size of the supported catalysts (6 nm). A similar effect has been reported for Mo-containing zeolites [34]. A different adsorbed carbon surface species with a stronger carbon-catalyst bond than for the unsupported catalysts might be possible as well. The presence of polyaromatic compounds inside SBA-15 pores cannot be ruled out, as observed in [35]. However, in the present case, the rate of ethylene formation was by a factor of 1000 higher than the rate for benzene and toluene formation (Fig. 10). Thus, it is more likely that the carbon surface species were CH_x instead of polyaromatic. The small CO₂ peak between 300 and 400 °C was observed in all samples, including the fresh catalysts. It most likely was a remnant of the copolymer.

The weight changes determined with TPO-TGA agreed with TPO-MS analyses, as summarized in Table S2 and S3. For example, GaN/SBA15-700 had 5.8 mg_C g_{cat}⁻¹ and 6.5 mg_{CH} g_{cat}⁻¹ based on TPO-MS and TPO-TGA, respectively. Ga₂O₃/SBA15 had 17.9 mg_C g_{cat}⁻¹ and 21.5 mg_{CH} g_{cat}⁻¹ based on TPO-MS and TPO-TGA, respectively. The results for the TPO-MS analyses were slightly lower, as it was based on CO₂ (i.e., carbon) only, whereas TPO-TGA was based on the weight loss (i.e., carbon and hydrogen included). Gerecke et al. reported much higher carbon depositions of

565 43 to 120 mg_C g_{cat}⁻¹ for the non-oxidative methane coupling to ethylene over PtSn-zeolite catalysts
566 [32].

567 Based on the TPO results, the overall carbon-based selectivities (i.e., C₂H₄, C₃H₈, C₆H₆, C₇H₈,
568 C₁₀H₈, and adsorbed carbon *C_{ads}*) were determined and summarized in Table 4 together with the
569 overall CH₄ conversion and C₂H₄ yield.

570 The nitridated support without any gallium (N-SBA15-800) did not exhibit any methane
571 activation, which was also evident from the color of the used catalyst, which was white same as
572 the fresh catalyst (not shown). All supported catalysts achieved a higher C₂H₄ overall selectivity
573 than the unsupported catalysts (43-70% vs. 30-49%). The GaN/SBA15-700 and 750 catalysts had
574 the highest C₂H₄ selectivity with 70%, but the lowest yields due to the lower CH₄ conversion.
575 However, the Ga₂O₃/SBA15 and GaN/SBA15-650 catalysts had a considerably higher adsorbed
576 carbon (coke) content. In addition, the Ga₂O₃/SBA15 produced a significant amount of carbon
577 oxides and water.

578 Less than 0.5 mol% of the total methane feed added was converted to adsorbed carbon (e.g., CH*
579 or CH₂*) within 7 h time on stream. After 7 h on stream, the adsorbed carbon to gallium molar
580 ratio was about $C_{ads}/Ga = 1 \pm 0.05$ for GaN/SBA15-650 and Ga₂O₃/SBA15. With increasing
581 nitridation temperature the ratio decreased to $C_{ads}/Ga = 0.25 \pm 0.05$ for the GaN/SBA15-700, -750
582 and -800 samples. For the nitridated samples, this might indicate that the adsorbed carbon species
583 (CH* or CH₂*) are site-selective [36]. Based on this, a Ga dispersion of approximately 25% can
584 be estimated for the supported catalyst that has GaN cluster sizes of 3-5 nm (from Fig. 4 B and
585 C).

586 The turnover frequency (TOF) could not be calculated as the active surface area (number of actives
 587 sites) could not be determined via standard chemisorption using CH₄ and CH₄-TPD techniques
 588 (not shown). CH₄ did not chemisorb at low temperatures (25-45 °C). Our DFT results [21]
 589 indicated that the first step of CH₄ activation involved weak adsorption on the *m*-plane of the GaN,
 590 with carbon weakly bonded to Ga, forming a Ga–C bond following the alkyl mechanism [18,21].
 591 A similar result was obtained for Ga₂O₃, with carbon bonded to Ga while one H attracted to O
 592 (alkyl mechanism) [21]. CH₄ can also adsorb via the carbenium mechanism [10] to form a methoxy
 593 group, Ga–O–CH₃; however, based on the DFT calculation, the carbenium mechanism was not
 594 favored. This was also in agreement with in-situ ¹³C solid-state NMR spectroscopy experiments
 595 conducted over Ga/H-BEA by Luzgin et al. [10]. They showed that gallium-methyl species
 596 (Ga–CH₃) was the major surface intermediate, and gallium-methoxy was only a minor surface
 597 species. Our DFT results implied that CH₄ did not adsorb on GaN and Ga₂O₃ as a molecule but
 598 through dissociative adsorption. This confirms that CH₄-TPD and CH₄ chemisorption techniques
 599 failed to determine the number of active sites at low temperatures. Based on the experimental
 600 results [33] as well as our reported DFT simulations [21], it is hypothesized that CH₄ undergoes
 601 fast dissociative adsorption on all the active sites (R1 to R3, Fig. 12) for GaN and Ga₂O₃. The
 602 active CH₃* surface intermediate is further dehydrogenated to CH₂* with the release of H₂ (R4
 603 and R5 in Fig. 12), which are the rate-determining steps, and then dimerized to C₂H₄. The CH₂
 604 surface intermediate can be further dehydrogenated to CH* and C* (R7, Fig. 12), which might
 605 lead to undesired coke. For the Ga₂O₃ catalysts, H₂O is formed via R3', leaving a vacant site (Fig.
 606 12B). The carbon oxides are produced from the interaction of adsorbed CH₂* (on Ga) with
 607 neighboring top layer oxygen atoms [21].

608 To summarize, catalyst nitridation was needed for two reasons: (1) over gallium oxide H_2O and
609 CO_x were formed in addition to C_2H_4 , leading to lower C_2H_4 selectivity ($S_{\text{C}_2\text{H}_4}$, Fig. 13), and (2)
610 nitridation reduced the carbon deposition (C_{ads} Fig. 13). Hence, nitridation improved the atom
611 conversion efficiency for CH_4 carbon, and the efficiency was higher for the supported catalyst. In
612 the case of unsupported catalysts, the nitridation temperature affects directly the nitrogen content
613 (i.e., Ga_2O_3 conversion); however, the degree of nitridation did not influence the methane activity
614 in terms of $S_{\text{C}_2\text{H}_4}$ and C_{ads} as a complete bulk nitridation was not needed (Fig. 13B). Surface
615 nitridation was sufficient for improving $S_{\text{C}_2\text{H}_4}$ and reducing C_{ads} . A similar behavior was observed
616 for the supported catalyst (except GaN/SBA15-650); in detail, with higher nitridation temperature
617 ($\geq 700^\circ\text{C}$) the total surface area decreased, which did not influence the activity in terms of $S_{\text{C}_2\text{H}_4}$
618 and C_{ads} (Fig. 13A). There is an additional factor of support basicity in GaN/SBA15 catalysts.
619 Huo et al. [37] have shown that nitridated N-SBA-16 support was more stable and had lower
620 carbon deposition than non-nitridated SBA-16 for Ni/SBA-16 catalysts for methane dry reforming.
621 Depending upon the nitridation temperature, the O atoms in SBA-16 and SBA-15 (silanol OH)
622 are replaced by N (NH_2) [37,38]. The increased basicity in N-SBA-16 resulted in stronger metal-
623 support interaction [37]. As reported by Chino et al. [38], in their work on SBA-15 nitridation, the
624 nitrogen uptake by SBA-15 was negligible below 700°C . The nitrogen content increased from 2
625 wt% to 16 wt% from 700°C to 1000°C [38]. This explains why our GaN/SBA15-650 had the
626 highest C_{ads} among all the supported nitride catalysts, as the SBA-15 support was not sufficiently
627 nitridated. From Fig. 13, it can be concluded that the optimum nitridation temperatures were 700°C
628 $^\circ\text{C}$ and 750°C for the supported and the unsupported catalysts, respectively.

4 Conclusions

For the first time, this work reported the synthesis and characterization of supported GaN/SBA15 catalysts for methane activation to ethylene. Additionally, unsupported GaN catalysts were also synthesized, characterized, and tested for methane activation. The effect of synthesis parameters and catalyst type were investigated on ethylene selectivity and carbon deposition on the catalysts. We addressed the issue of carbon deposition by using a less acidic support. The catalysts produced more ethylene than aromatics and less coke when compared to precious metal and metal oxide catalysts. The unsupported and SBA-15 supported gallium nitride catalysts were synthesized via a simple one-pot procedure and incipient impregnation, respectively, followed by calcination and subsequent nitridation. The influence of the nitridation condition on the catalyst structure and further on the direct non-oxidative methane activation was investigated. With higher nitridation temperature, the Ga_2O_3 conversion to GaN of the unsupported samples increased from 35 to 88%, while the surface area decreased significantly from 19 to $11 \text{ m}^2 \text{ g}^{-1}$. For the supported catalyst, the Ga_2O_3 conversion to GaN could not be determined; however, since the gallium particles inside SBA-15 pores were around 3-5 nm (from Fig. 4 B and C), high conversions can be assumed. The total surface area of the supported gallium samples was much larger, which decreased from 420 to $320 \text{ m}^2 \text{ g}^{-1}$ with increasing nitridation temperature.

The unsupported GaN catalysts deactivated rather fast within 3 h, whereas the supported GaN/SBA catalysts were stable and exhibited a steady H_2 and hydrocarbons formation rate for 7 h. The main hydrocarbon product was C_2H_4 , with selectivities of up to 71 mol% for the supported and 50 mol% for the unsupported samples. The balance was predominantly adsorbed surface carbon and coke. The supported catalysts had 10 times higher C_2H_4 and H_2 formation rate per gram of Ga than the unsupported catalysts. Ga_2O_3 and $\text{Ga}_2\text{O}_3/\text{SBA15}$ samples had a smaller C_2H_4 selectivity as they

produced a significant amount of H₂O and CO₂ through the reaction of the lattice oxygen with CH₄. This was not observed for the nitridated catalysts, even for the GaN-650 sample that contained ~65 % Ga₂O₃.

Higher surface area, well-dispersed GaN in the supported catalysts increased the accessibility of CH₄ to the active sites (GaN). The accessibility to GaN was much lower in practically non-porous unsupported catalysts (even with higher Ga content). In conclusion, based on $S_{C_2H_4}$ and C_{ads} , the catalyst of interest for methane activation and coupling to ethylene is the supported catalyst GaN/SBA15-700.

Supporting information

Comparison between GC and MS results for CH₄, H₂, and C₂H₄ (Fig. S1). Reproducibility results (Fig. S2). Nitrogen adsorption/desorption analysis (Fig. S3 and S9). TEM images (Fig. S4 to S8 and S10). Mass spectra analysis for unsupported catalyst (Fig. S11 and S12). SEM-EDS for fresh Ga₂O₃ (Fig. S13) and spent Ga₂O₃ (Fig. S14). XRD for fresh Ga₂O₃ and spent Ga₂O₃ (Fig. S15). Naphthalene formation rate over unsupported gallium catalyst (Fig. S16). Pictures of fresh and used catalysts (Fig. S17). Ratio of H₂ and C₂H₄ formation rates (Fig. S18). Water evolution during TPO-MS (Fig. S19). TPO-TGA results for spent and fresh catalysts (Fig. S20). Equilibrium conversion of CH₄ and yields of C₂H₄ and C₂H₆ as a function of temperature (Fig. S21). CO₂ and H₂O formation rate of Ga₂O₃/SBA15 and GaN/SBA15-650 (Fig. S22). XRD for spent catalysts (Fig. S23). Adsorbed carbon on spent catalyst (Table S1–3).

Acknowledgments

The authors thank Aleksandra Djuric for conducting the N₂ adsorption/desorption and Ranjan Roy and Andrew Golsztajn for the ICP-OES measurements and helping authors for developing the total

nitrogen analysis method. The authors also thank Daniel Pacheco Gutierrez and Obinna Kingsley Uwa for their help with the catalyst synthesis. The authors also thank Mohsen Shahryari for his help with proofreading. J. Kopyscinski acknowledges the financial support from Fonds de recherche du Québec – Nature et technologies (FRQNT, Team Grant PR–253397) and via the Centre in Green Chemistry and Catalysis (FRQNT–2020-RS4–265155-CCVC) as well as from Imperial Oil University Research Award and Natural Sciences and Engineering Research Council of Canada (NSERC CRDPJ 534026). CJ. Li thanks NSERC, Canada Research Chair, and the Fessenden Professorship of McGill University for support of this research.

References

- [1] K. Patel, IBISWorld Industry Report 32511 Petrochemical Manufacturing in the US, 2019.
- [2] N. Leach, IBIS World Industry Report 32511CA Petrochemical Manufacturing in Canada, 2018.
- [3] C. Karakaya, R.J. Kee, Prog. Energy Combust. Sci. 55 (2016) 60–97.
- [4] S. Ma, X. Guo, L. Zhao, S. Scott, X. Bao, J. Energy Chem. 22 (2013) 1–20.
- [5] P. Tang, Q. Zhu, Z. Wu, D. Ma, Energy Environ. Sci. 7 (2014) 2580.
- [6] J.J. Spivey, G. Hutchings, Chem. Soc. Rev. 43 (2014) 792–803.
- [7] S. Ma, X. Guo, L. Zhao, S. Scott, X. Bao, J. Energy Chem. 22 (2013) 1–20.
- [8] D. Gerceker, A. Hussain Motagamwala, K.R. Rivera-Dones, J.B. Miller, G.W. Huber, M. Mavrikakis, J.A. Dumesic, ACS Catal. 7 (2017) 2088–2100.
- [9] E. Mansoor, M. Head-Gordon, A.T. Bell, ACS Catal. 8 (2018) 6146–6162.
- [10] M. V. Luzgin, A.A. Gabrienko, V.A. Rogov, A. V. Toktarev, V.N. Parmon, A.G. Stepanov, J. Phys. Chem. C 114 (2010) 21555–21561.
- [11] D. Gerceker, A.H. Motagamwala, K.R. Rivera-Dones, J.B. Miller, G.W. Huber, M. Mavrikakis, J.A. Dumesic, ACS Catal. 7 (2017) 2088–2100.
- [12] Y. Xiao, A. Varma, ACS Catal. 8 (2018) 2735–2740.
- [13] D. Bajec, A. Kostyniuk, A. Pohar, B. Likozar, Int. J. Energy Res. 43 (2019) 6852–6868.
- [14] H. Sheng, E.P. Schreiner, W. Zheng, R.F. Lobo, ChemPhysChem 19 (2018) 504–511.

- 702 [15] X. Guo, G. Fang, G. Li, H. Ma, H. Fan, L. Yu, C. Ma, X. Wu, D. Deng, M. Wei, D. Tan,
703 R. Si, S. Zhang, J. Li, L. Sun, Z. Tang, X. Pan, X. Bao, *Science*. 344 (2014) 616–619.
- 704 [16] J.S.J. Hargreaves, *Coord. Chem. Rev.* 257 (2013) 2015–2031.
- 705 [17] L. Li, S. Fan, X. Mu, Z. Mi, C.-J. Li, *J. Am. Chem. Soc.* 136 (2014) 7793–7796.
- 706 [18] L. Li, X. Mu, W. Liu, X. Kong, S. Fan, Z. Mi, C.J. Li, *Angew. Chemie - Int. Ed.* 53
707 (2014) 14106–14109.
- 708 [19] C.-J. Li, Z. Mi, L. Li, Process for Producing Aromatic Compounds Using Light Alkanes,
709 PCT/CA2014/050864, 2015.
- 710 [20] K. Dutta, L. Li, P. Gupta, D.P. Gutierrez, C.-J. Li, J. Kopyscinski, *Catal. Commun.* 106
711 (2018) 16–19.
- 712 [21] V. Chaudhari, K. Dutta, C.-J. Li, J. Kopyscinski, *Mol. Catal.* In-print (2019).
- 713 [22] D. Zhao, J. Feng, Q. Huo, N. Melosh, G.H. Fredrickson, B.F. Chmelka, G.D. Stucky,
714 *Science*. 279 (1998) 548–552.
- 715 [23] I. Barin, O. Knacke, O. Kubaschewski, *Thermochemical Properties of Inorganic*
716 *Substances*, Springer Berlin Heidelberg, Berlin, Heidelberg, 1977.
- 717 [24] W.-S. Jung, *Mater. Lett.* 57 (2002) 110–114.
- 718 [25] A.-H. Lu, F. Schüth, *Adv. Mater.* 18 (2006) 1793–1805.
- 719 [26] S.N. Talapaneni, D. Park, J. Choy, K. Ramadass, A. Elzatahry, A.S. Al Balawi, A.M. Al-
720 Enizi, T. Mori, A. Vinu, *Chem. Sel.* 1 (2016) 6062–6068.
- 721 [27] S. Geller, *J. Chem. Phys.* 33 (1960) 676–684.
- 722 [28] E. Auer, A. Lugstein, S. Löffler, Y.J. Hyun, W. Brezna, E. Bertagnolli, P. Pongratz,
723 *Nanotechnology* 20 (2009) 434017.
- 724 [29] P. Ravadgar, R.-H. Horng, S.-D. Yao, H.-Y. Lee, B.-R. Wu, S.-L. Ou, L.-W. Tu, *Appl.*
725 *Phys. Lett.* 67 (1995) 2914–2919.
- 726 [30] B. Xu, B. Zheng, W. Hua, Y. Yue, Z. Gao, *J. Catal.* 239 (2006) 470–477.
- 727 [31] C. Guizani, F.J. Escudero Sanz, S. Salvador, *Comptes Rendus Chim.* 19 (2016) 423–432.
- 728 [32] D. Gerceker, A.H. Motagamwala, K.R. Rivera-Dones, J.B. Miller, G.W. Huber, M.
729 Mavrikakis, J.A. Dumesic, *ACS Catal.* 7 (2017) 2088–2100.
- 730 [33] K. Dutta, M. Shahryari, J. Kopyscinski, *Ind. Eng. Chem. Res.* (2019) In-print.
- 731 [34] N. Kosinov, E.A. Uslamin, F.J.A.G. Coumans, A.S.G. Wijkema, R.Y. Rohling, E.J.M.
732 Hensen, *ACS Catal.* 8 (2018) 8459–8467.

- 733 [35] N. Kosinov, A.S.G. Wijpkema, E. Uslamin, R. Rohling, F.J.A.G. Coumans, B. Mezari, A.
734 Parastaev, A.S. Poryvaev, M. V. Fedin, E.A. Pidko, E.J.M. Hensen, *Angew. Chemie Int.*
735 *Ed.* 57 (2018) 1016–1020.
- 736 [36] J. Van Doorn, J.A. Moulijn, *Catal. Today* 7 (1990) 257–266.
- 737 [37] M. Huo, L. Li, X. Zhao, Y. Zhang, J. Li, *J. Fuel Chem. Technol.* 45 (2017) 172–181.
- 738 [38] N. Chino, T. Okubo, *Microporous Mesoporous Mater.* 87 (2005) 15–22.
- 739

List of Tables

- Table 1. Nitrogen adsorption and desorption results for unsupported Ga_2O_3 , GaN catalysts.
- Table 2. Nitrogen adsorption and desorption results for supported Ga_2O_3 , GaN catalysts on SBA-15 (NH_3 exposure time: 24 h).
- Table 3. Overall and hydrocarbon (HC) selectivity, CH_4 conversion, and C_2H_4 yield for unsupported catalysts.
- Table 4. Overall and hydrocarbon selectivity for supported catalysts.

List of Figures

- Fig. 1. Results for nitridation of unsupported catalysts. (A) H_2O signal as a function of nitridation time at different temperatures, (B) Conversion of Ga_2O_3 as a function of temperature (C), XRD pattern as a function of temperature. (D) H_2O signal as function of nitridation time at 750°C , (E) Conversion of Ga_2O_3 as a function of nitridation time at 750°C and (F) XRD pattern as a function of nitridation time at 750°C .
- Fig. 2. HRTEM image of (A) fresh Ga_2O_3 and (B) fresh GaN-650 catalyst with GaN/ Ga_2O_3 intersection. Top left inset darkfield image at low resolution and top right inset electron diffraction pattern. (C) EDS analyses (Ga normalized) for Ga_2O_3 , fresh, and used GaN-650. Note: The green dashed line indicates approximately the boundary between GaN and Ga_2O_3 . Note: Cu and some of the C signals in EDS are from the grid.
- Fig. 3. Results for nitridation of supported catalysts. (A) H_2O signal and (B) XRD pattern as a function of nitridation temperature.
- Fig. 4. STEM image of (A) fresh $\text{Ga}_2\text{O}_3/\text{SBA15}$ and (B) fresh GaN/SBA15-650 catalyst. Top left inset HRTEM image and top right inset electron diffraction pattern. (C) fresh GaN/SBA15-800 catalyst. Top left inset HRTEM image and top right inset electron diffraction pattern. (D) Si normalized EDS analyses for $\text{Ga}_2\text{O}_3/\text{SBA15}$, fresh, and used GaN/SBA15-650. Note: Cu and some of the C signals in EDS are from the grid.
- Fig. 5. Normalized mass spectra as function of time for Ga_2O_3 (A to D) and GaN-750 (E to H) for mass to charge ratios of $m/z = 2$ (H_2 , red), $m/z = 18$ (H_2O , blue), $m/z = 28$ ($\text{C}_2\text{H}_4 + \text{CO}$, orange) and $m/z = 44$ (CO_2 , grey).
- Fig. 6. (A) Methane conversion and product flow rates of (B) hydrogen, (C) ethylene (D) propylene (E) benzene and (F) toluene as a function of time on stream for the methane activation at 700°C and 1 bar over unsupported Ga_2O_3 and GaN catalysts nitridated at different temperatures.
- Fig. 7. (A) Methane conversion and product flow rates of (B) hydrogen (C) ethylene (D) propylene (E) benzene and (F) toluene as a function of time on stream for methane activation carried out using unsupported GaN catalysts nitridated at 750°C at different ammonia exposure times (B). Methane activation conditions: 700°C and 1 bar.
- Fig. 8. TPO for spent unsupported GaN and Ga_2O_3 catalysts used for methane activation at 700°C .
- Fig. 9. Normalized mass spectra as function of time for $\text{Ga}_2\text{O}_3/\text{SBA15}$ (A to D), and GaN/SBA15-750 (E to H) for mass to charge ratios of $m/z = 2$ (H_2 , red), $m/z = 18$ (H_2O , blue), $m/z = 28$ ($\text{C}_2\text{H}_4 + \text{CO}$, orange) and $m/z = 44$ (CO_2 , grey).

Fig. 10. (A) Methane conversion and product flow rates of (B) hydrogen, (C) ethylene, (D) propylene, (E) benzene, and (F) toluene formation rates as a function of time on stream over supported Ga₂O₃ and GaN catalyst at different nitridation temperatures. Methane activation conditions: 700 °C and 1 bar.

Fig. 11. TPO for spent supported GaN/Ga₂O₃ on SBA-15 catalyst used for methane activation at 700 °C.

Fig. 12. Proposed underlying mechanism for methane dehydrogenation to ethylene over (A) GaN and (B) Ga₂O₃.

Fig. 13. Effect of nitridation on ethylene selectivity ($S_{C_2H_4}$) and adsorbed carbon (C_{ads}) on (A) unsupported GaN and (B) supported GaN/SBA15 catalysts. The dotted lines are for guidance only.

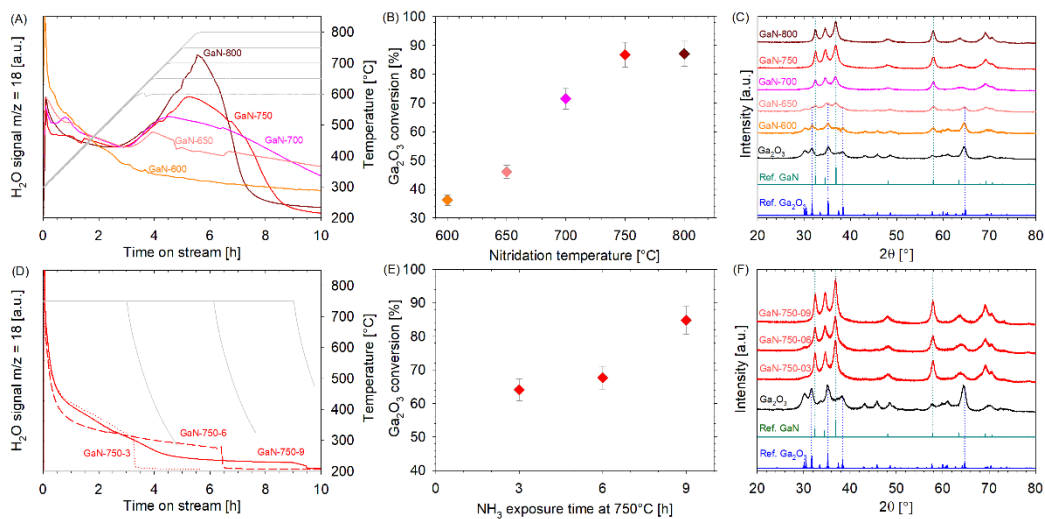


Fig. 1

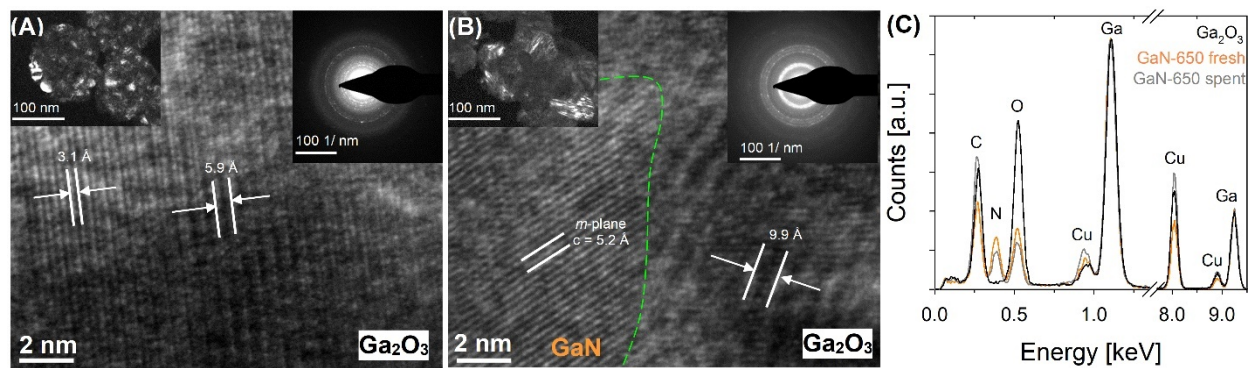


Fig. 2

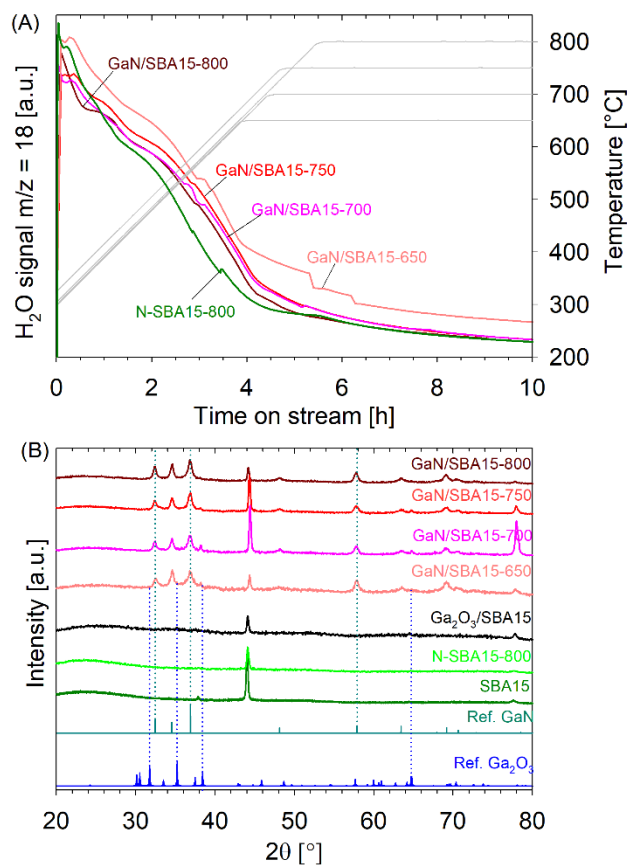


Fig. 3

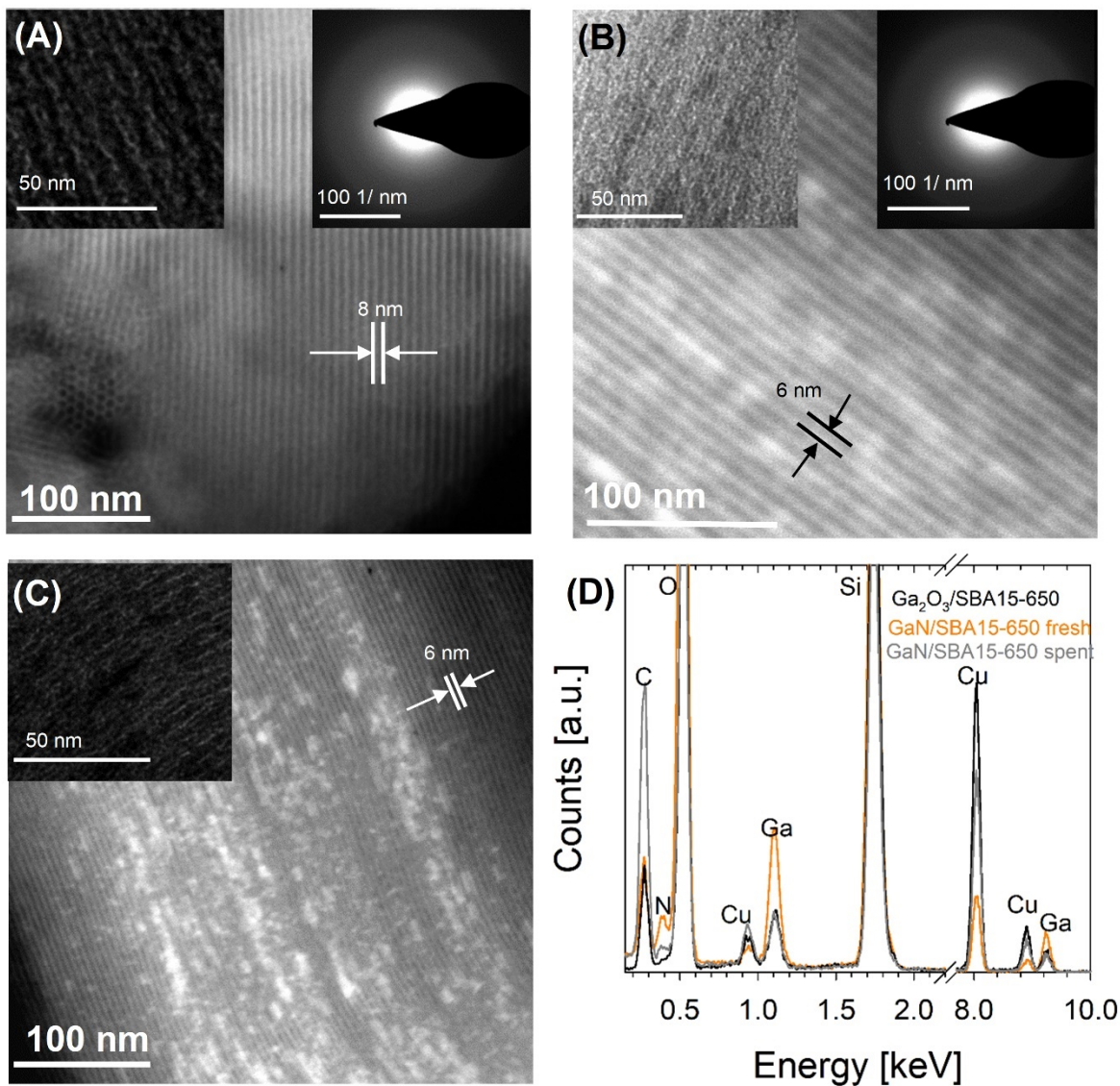


Fig. 4

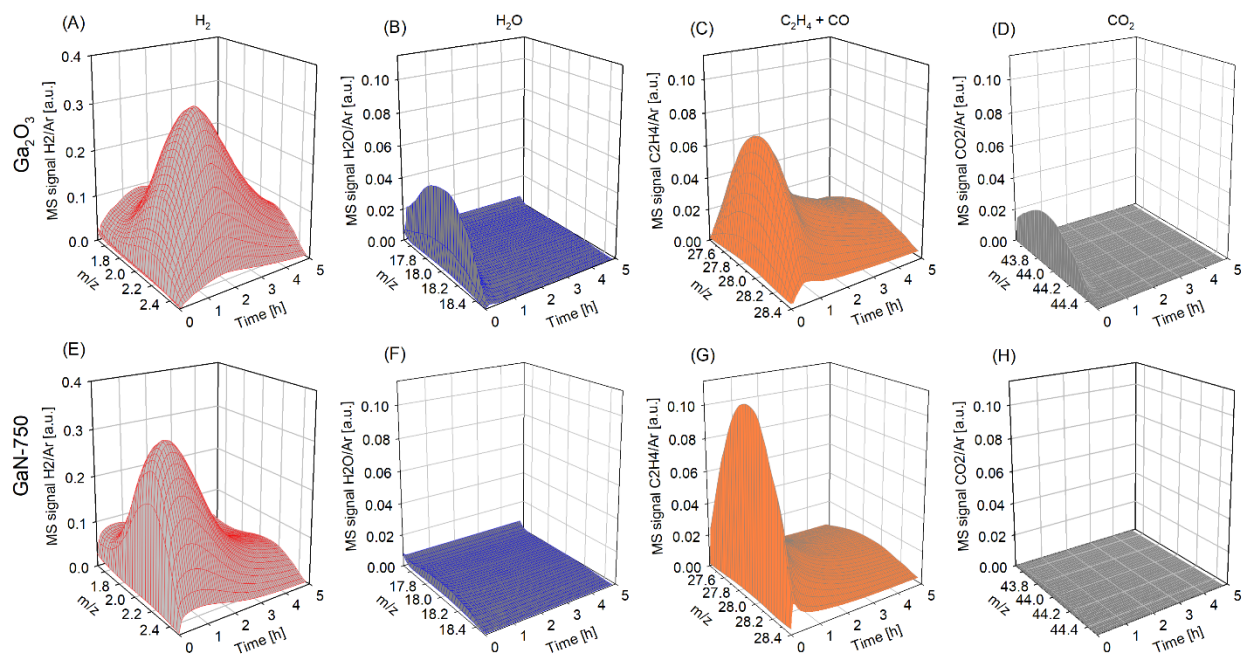


Fig. 5

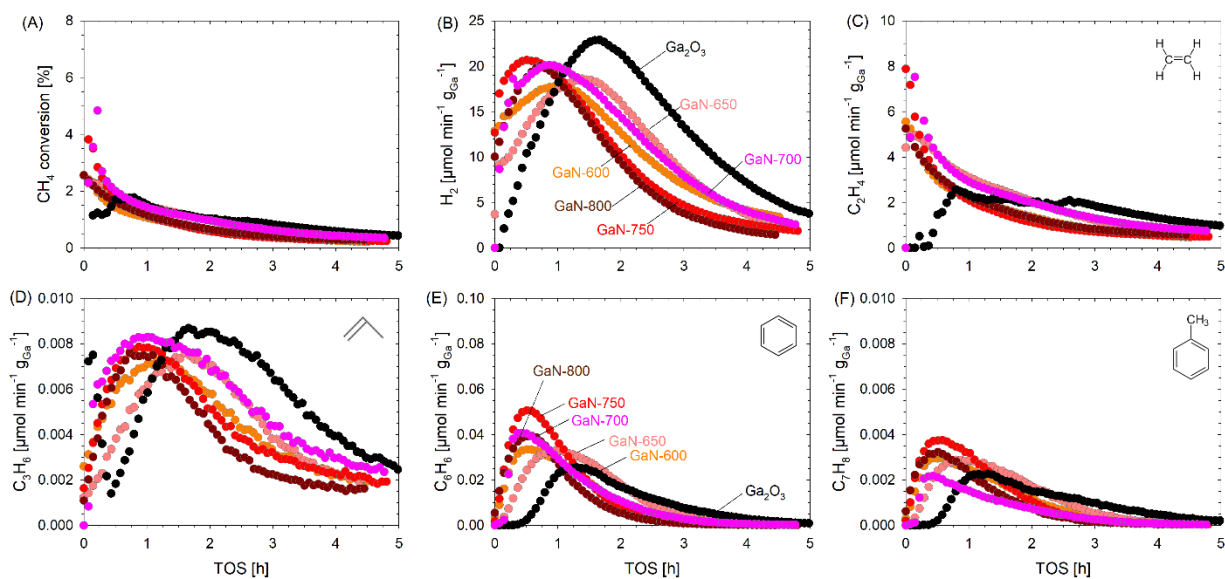


Fig. 6

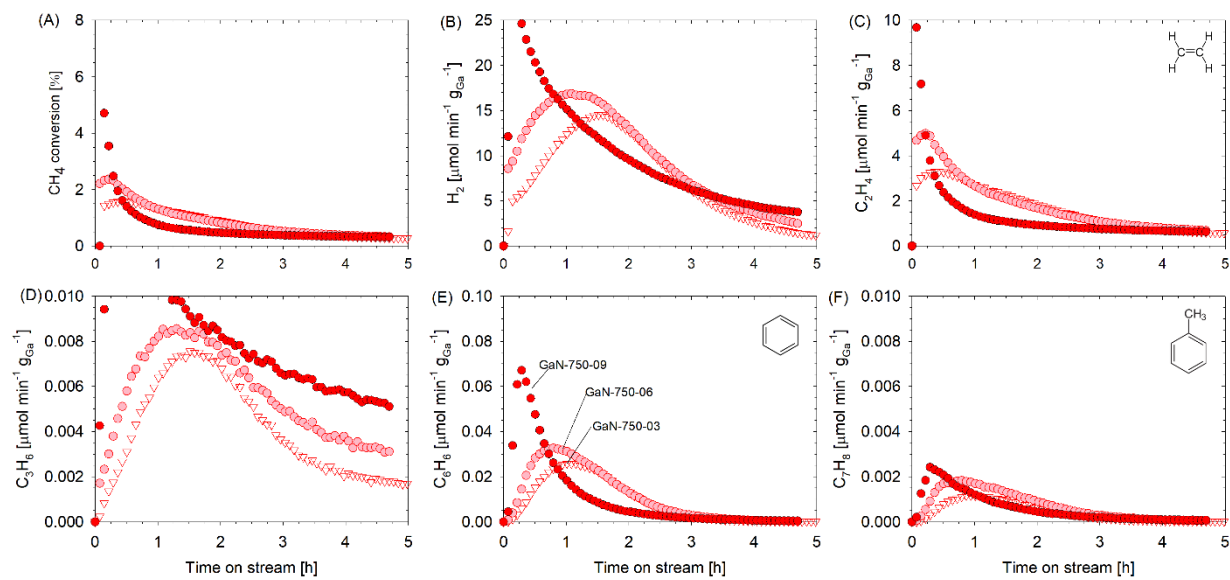


Fig. 7

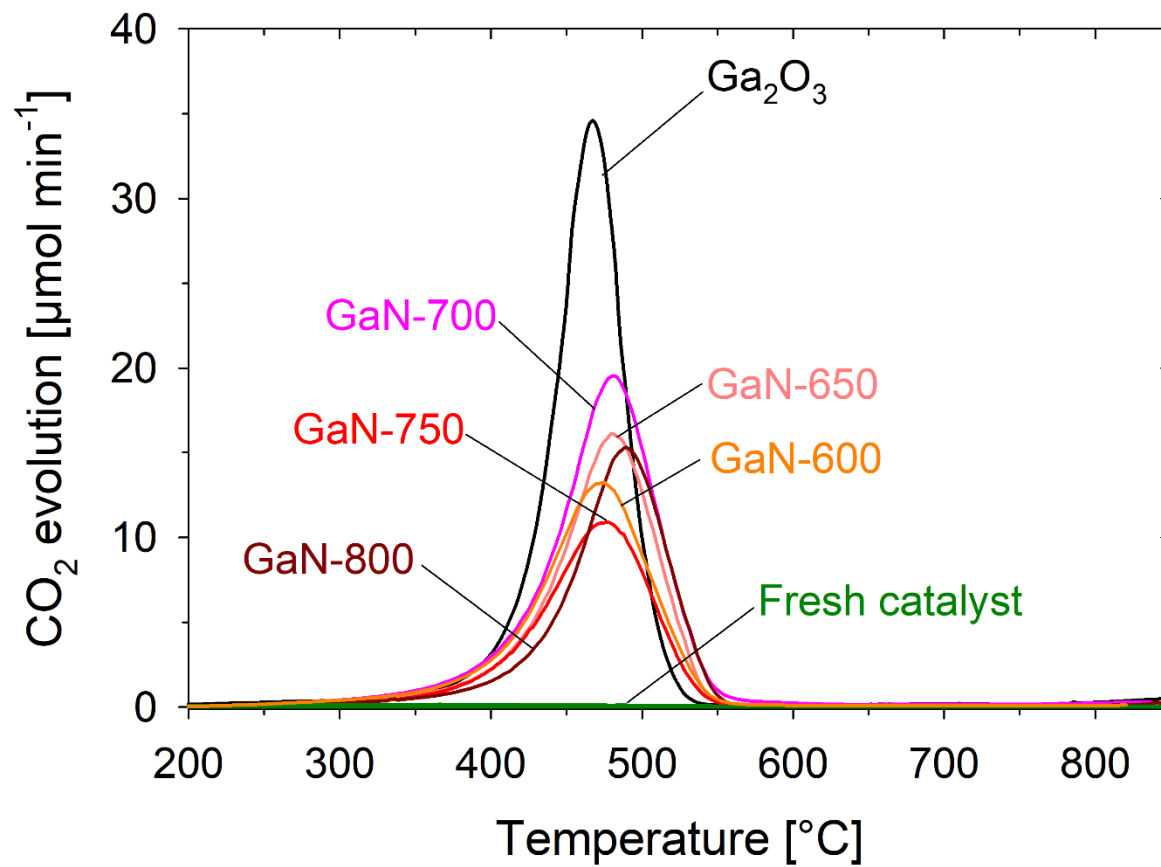


Fig. 8

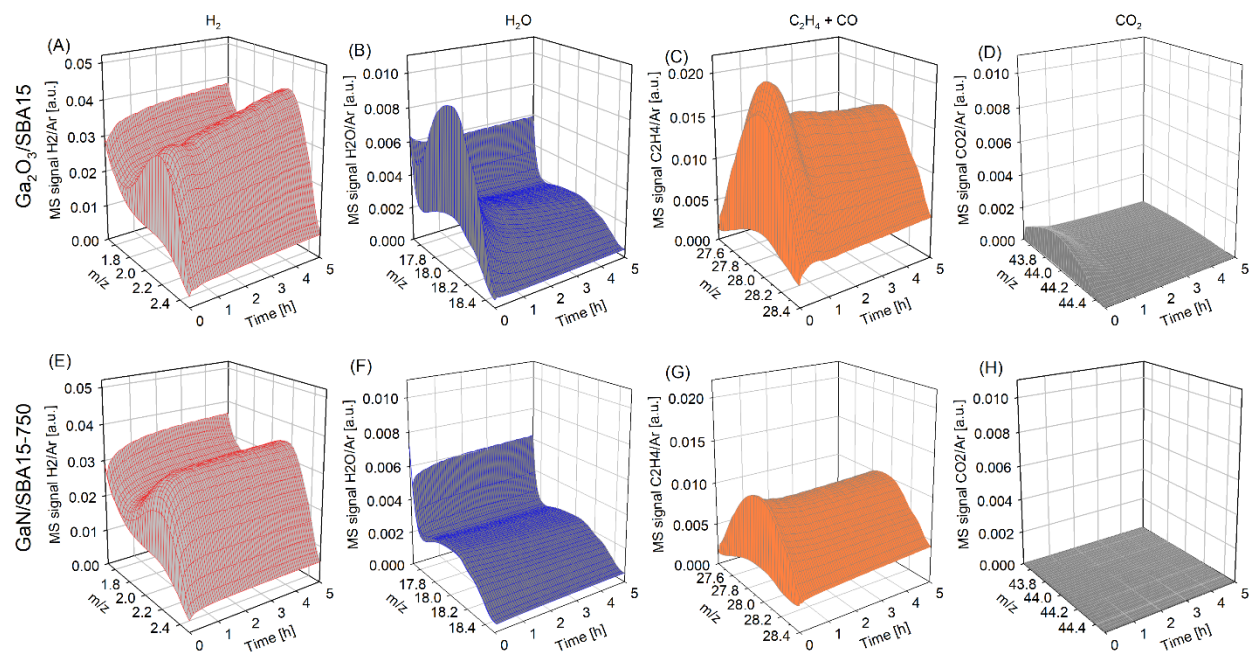


Fig. 9

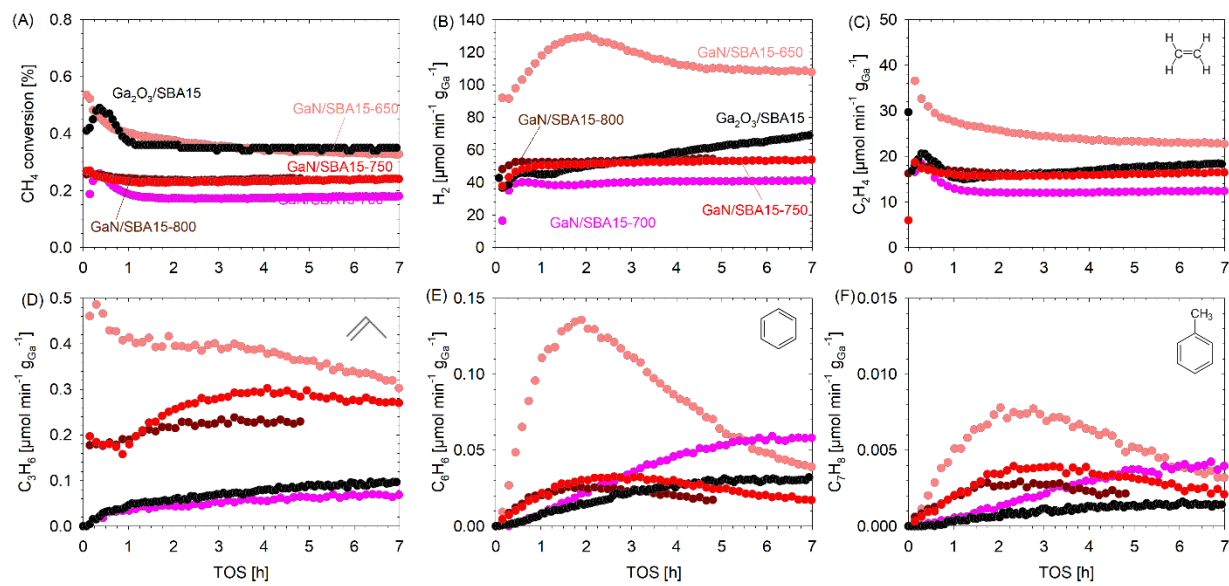


Fig. 10

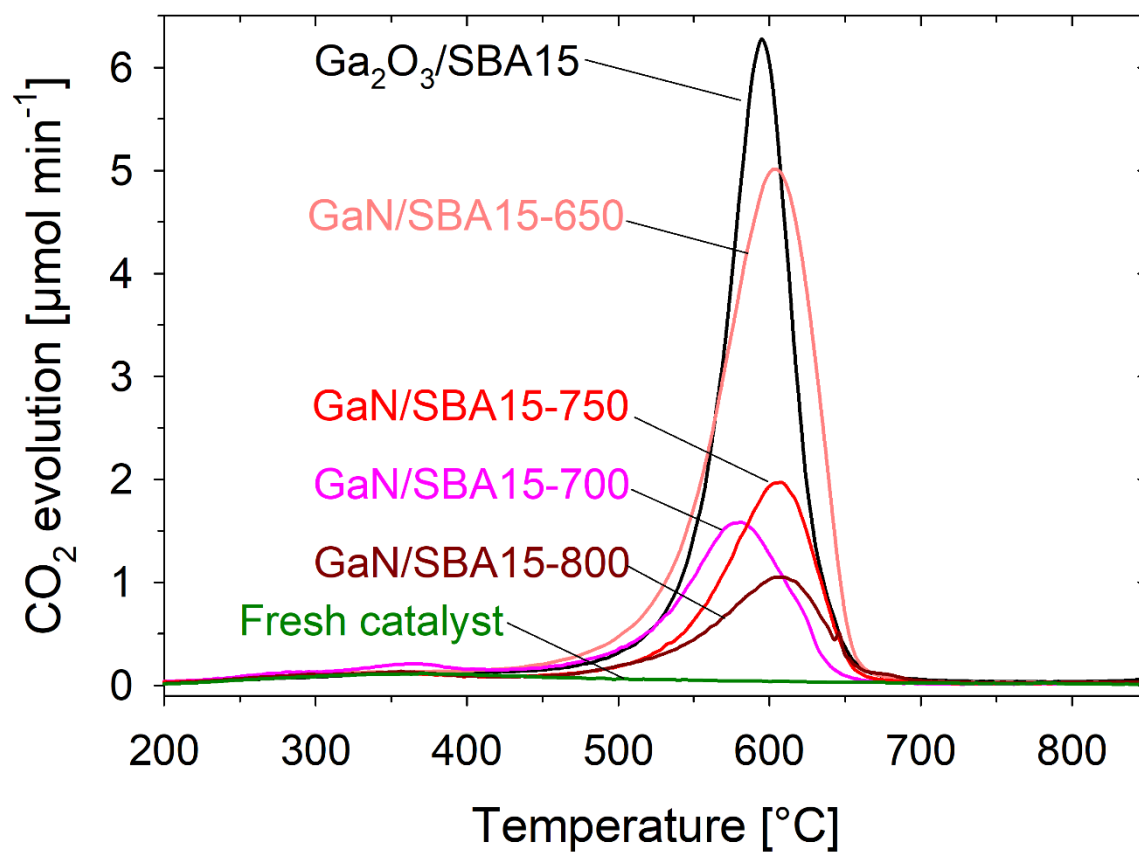
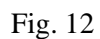


Fig. 11



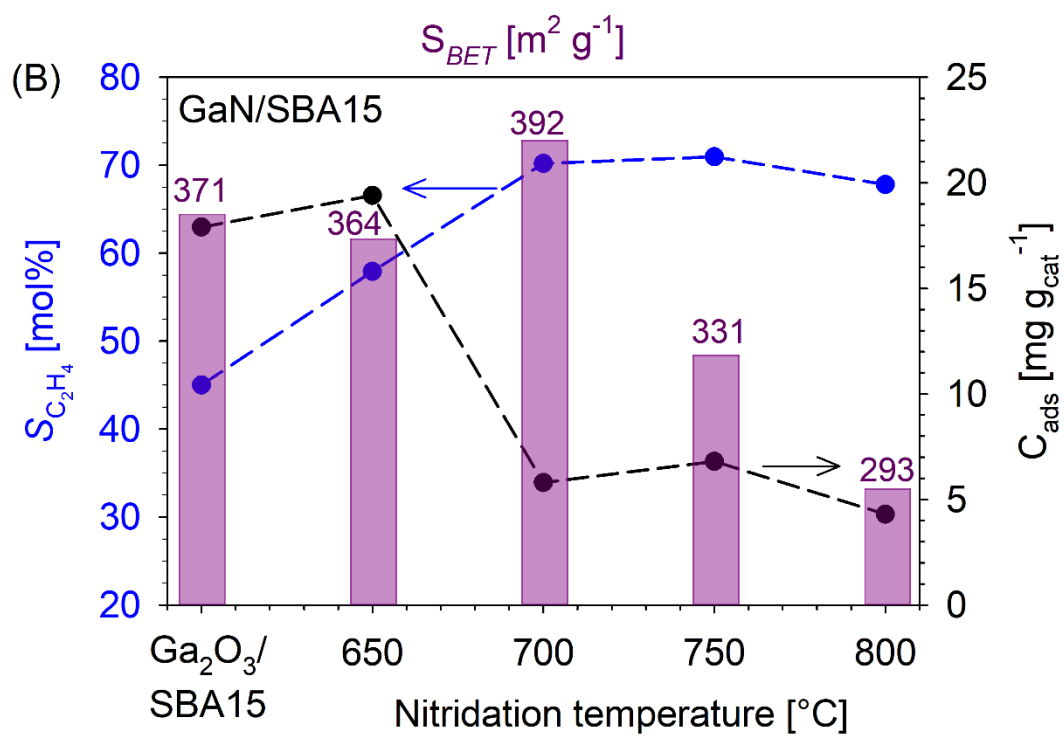
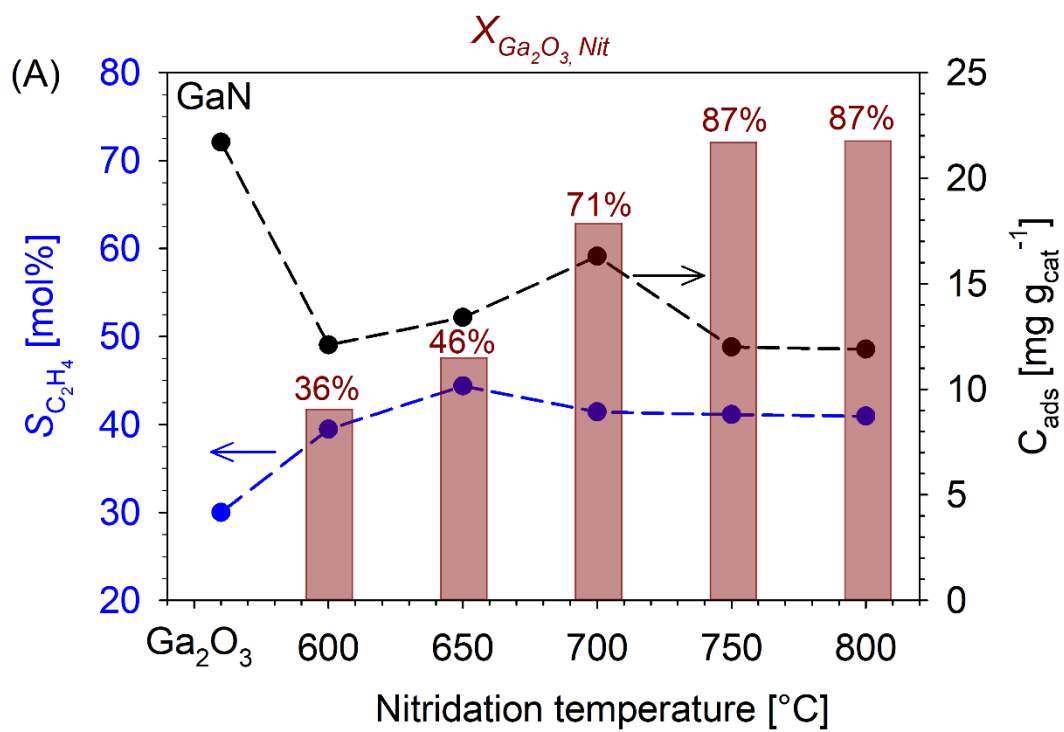


Fig. 13